INVESTIGATION OF EFFECTS OF INFILL PATTERN ON FATIGUE LIFE OF 3D-PRINTED COMPOSITE

A THESIS SUBMITTED TO
THE SCHOOL OF GRADUATE STUDIES.
OF
UNIVERSITY OF TURKISH AERONAUTICAL ASSOCIATION

BY

Jackson SAABA

IN PARTIAL FULFILLMENT OF THE REQUIREMENTS
FOR
THE DEGREE OF MASTER OF SCIENCE
IN
MECHANICAL AND AERONAUTICAL ENGINEERING

AUGUST 2024

INVESTIGATION OF EFFECTS OF INFILL PATTERN ON FATIGUE LIFE OF 3D-PRINTED COMPOSITE

A THESIS SUBMITTED TO
THE SCHOOL OF GRADUATE STUDIES.
OF
UNIVERSITY OF TURKISH AERONAUTICAL ASSOCIATION

BY

Jackson SAABA

IN PARTIAL FULFILLMENT OF THE REQUIREMENTS
FOR
THE DEGREE OF MASTER OF SCIENCE
IN
MECHANICAL AND AERONAUTICAL ENGINEERING

SUPERVISOR: Assoc. Prof. Dr. Hamit TEKİN

AUGUST 2024

Approval of the thesis:

INVESTIGATION OF EFFECTS OF INFILL PATTERN ON FATIGUE LIFE OF 3-DPRINTED COMPOSITE

submitted by **JACKSON SAABA** in partial fulfilment of the requirements for the degree of **Master of Science in Mechanical and Aeronautical Engineering, University of Turkish Aeronautical Association** by,

Assoc. Prof. Dr. Adnan GÜZEL
Dean, The School of Graduate Studies, UTAA _____

Assoc. Prof. Dr. Hamit TEKIN
Head of The Department,
Mechanical and Aeronautical Engineering, UTAA _____

Assoc. Prof. Dr. Hamit TEKIN
Supervisor: Mechanical engineering, UTAA _____

Examining Committee Members:

Assoc. Prof. Dr. Hamit TEKIN
Mechanical engineering,
University of Turkish Aeronautical Association _____

Assoc. Prof. Dr. Rahim JAFARI
Mechanical engineering,
University of Turkish Aeronautical Association _____

Asst. Prof. Dr. Ferit SAIT

Mechanical engineering, Çankaya University _____

Date: 02 August 2024

I hereby declare that all information in this document has been obtained and presented in accordance with academic rules and ethical conduct. I also declare that, as required by these rules and conduct, I have fully cited and referenced all material and results that are not original to this work.

Jackson SAABA

ABSTRACT

INVESTIGATION OF EFFECTS OF INFILL PATTERN ON FATIGUE LIFE OF 3D-PRINTED COMPOSITE

Jackson, SAABA
Master of Science, Mechanical and Aeronautical Engineering
Supervisor: Assoc. Prof. Dr. Hamit Tekin

August 2024, 69 pages

The emergence of 3D printing has brought about a new era in producing prototypes, construction materials, machine components, and other items. This thesis investigated the effects of topology optimization on the fatigue life of 3D-printed composite. Our goal was to improve the structural performance and durability of these composites, which are being utilized in more and more high-performance applications, by utilizing cutting-edge computational techniques. In this research, many optimum topologies are thoroughly analyzed, manufactured using additive manufacturing techniques, and then fatigue tested. Our research shows that topology optimization can greatly increase the fatigue resistance of composites that are 3D printed, offering important new information for manufacturing and design procedures in the future. This work contributes to our understanding of fatigue behavior in optimized structures and provides useful advice for designing composite parts with increased durability. The infill used in 3D printing reduces the amount of material required, which shortens the printing time while preserving the aesthetic appeal of the final product. The fatigue life of 3D-printed composite materials following infill patterns is assessed using ANSYS software. The material was added to engineering data via static structure and exported to the design module for meshing and loading for the fatigue analysis.

Keywords: Infill patterns, Fatigue life, Additive manufacturing, FDM, Composite materials.

ÖZ

DOLGU DESENİNİN 3D BASKILI KOMPOZİTİN YORULMA ÖMRÜ ÜZERİNDEKİ ETKİLERİNİN İNCELENMESİ

Jackson, SAABA
Yüksek Lisans, Makina ve Uçak Mühendisliği
Tez Yöneticisi: Assoc. Prof. Dr. Hamit TEKIN

August 2024, 69 pages

3D baskının ortaya çıkışı, prototipler, inşaat malzemeleri, makine bileşenleri ve diğer öğelerin üretiminde yeni bir çağ getirdi. Bu tez, topoloji optimizasyonunun 3D baskılı kompozitin yorulma ömrü üzerindeki etkilerini araştırmıştır. Amacımız, giderek daha yüksek performanslı uygulamalarda kullanılan bu kompozitlerin yapısal performansını ve dayanıklılığını, en son hesaplama tekniklerini kullanarak iyileştirmekti. Bu araştırmada, birçok optimum topoloji kapsamlı bir şekilde analiz edilmiş, eklemeli üretim teknikleri kullanılarak üretilmiş ve ardından yorulma testi yapılmıştır. Araştırmamız, topoloji optimizasyonunun 3D baskılı kompozitlerin yorulma direncini büyük ölçüde artırabileceğini ve gelecekte üretim ve tasarım prosedürleri için önemli yeni bilgiler sunabileceğini gösteriyor. Bu çalışma, optimize edilmiş yapılardaki yorulma davranışını anlamamıza katkıda bulunur ve daha fazla dayanıklılığa sahip kompozit parçalar tasarlamak için faydalı tavsiyeler sağlar. 3D baskıda kullanılan dolgu, gereken malzeme miktarını azaltır, bu da nihai ürünün estetik çekiciliğini korurken baskı süresini kısaltır. Dolgu desenlerini takip eden 3D baskılı kompozit malzemelerin yorulma ömrü, ANSYS yazılımı kullanılarak değerlendirilir. Malzeme, statik yapı aracılığıyla mühendislik verilerine eklendi ve yorulma analizi için ağ oluşturma ve yükleme için tasarım modülüne aktarıldı.

Anahtar Kelimeler: dolgu desenleri, Yorulma ömrü, Eklemeli imalat, FDM, Kompozit malzemeler.

ACKNOWLEDGMENTS

I would like to give my sincere thanks to my supervisor Assoc. Prof. Dr. Hamit Tekin for his knowledge, guidance, support, encouragement and motivation. I would like to thank my thesis examiner committee members Assoc. Prof. Dr. Rahim Jafari and Asst. Prof. Dr. Ferit Sait for their encouragement and helpful comments. I would like to thank to my lab mate salen for her introduction on 3D-printing technology.

I would like to give thankful to my classmates especially Syd for his help.

I thank Dean's secretary Eda for her help with kindness.

TABLE OF CONTENTS

LIST OF TABLES

TABLES

LIST OF FIGURES

FIGURES

CHAPTER 1

INTRODUCTION

1.1 Additive Manufacturing

Unlike traditional subtractive manufacturing processes that remove material from a solid block, additive manufacturing adds material where needed, building up the object layer by layer. In additive manufacturing, an object is created layer by layer, each layer represents a thinly sliced horizontal cross-section of the finished product [1, 2]. Making a digital 3D model of the product to be made is the first step in the process. Typically, the model is designed using computer-aided design (CAD) software. Materials from diverse sources, such as metals, ceramics, and polymers materials, are used in additive manufacturing. Layer by layer, these materials are applied under the digital design's parameters [3]. The three well-known techniques for additive manufacturing FDM, SLA, and SLS each have special qualities and benefits that make them appropriate for a variety of uses. Knowing the ins and outs of each technique makes it easier to choose the right technology for a particular project, guaranteeing the best possible outcomes in terms of mechanical performance, surface polish, and material qualities [1, 4]. numerous industries, such as aerospace, automotive, healthcare, architecture, and consumer goods are extensively utilize additive manufacturing [5, 6].

Compared to traditional production methods, additive manufacturing offers numerous benefits, such as flexibility in Design, Bespoke designs, and intricate geometries that are easily constructed [7]. Prototyping and iterative design happen quickly and material waste is reduced as only the necessary amount is used [1, 4, 8].

1.2 Motivation

This study investigated the effect of infill densities and patterns in part made with the Fused Deposition Modeling using carbon fiber reinforced polyamide PA12CF, ABS, and PLA. It was found that infill density and structures have a major impact on the mechanical properties. In [9] Test pieces reinforced with lightweight carbon fiber were utilized to ascertain the impact of infill patterns on mechanical characteristics. [9], According to this study, the relative flexural modulus was influenced by the material's relative density. Additionally, the study examined the properties of infill constructions, including the experimental and theoretical masses of 3D printed components at various infill ratios. The specimens with larger masses showed good tensile qualities. Furthermore, the investigation of mechanical properties of typical infills, and topology optimization was performed to minimize the material volume and improve load-carrying capacity. 3D printing, also known as additive manufacturing (AM), is a rapidly advancing manufacturing technique that enables the production of intricate geometric structures and physical models with high precision and at a low cost [10]. Although composite 3D printing is still in its early stages, it has the potential to revolutionize the industry. According to a survey by smart tech analysis, the global market for 3D printed composites is expected to reach around $10 billion within the next ten years[11], [12].

1.3 Proposed Methods

In this study, the effect of infill density and infill pattern on fatigue life of 3D printed parts subjected to uniaxial fluctuating tensile loading is investigated through ANSYS Workbench.

The process involved exporting the CAD model as a stereolithographic format (STL) and importing it into ANSYS. For each case, 9 model constants were obtained. Consideration was given to both non-reinforced thermoplastics (PLA and ABS) and reinforced thermoplastics PA12CF. Tensile and fatigue tests were used to evaluate the properties of materials to provide precise input data for simulations.

This study has analyzed the impact on the structural performance of various infill patterns and densities (rectilinear, triangular, honeycomb, 25%, 60%, and 95%). The filling densities and filling patterns are essential for striking a balance between material savings and weight reduction. For in-depth finite element analysis, the dog bone shape models with various infill patterns and densities were generated in Solid Works and loaded into the ANSYS workbench. The models meshed at a certain meshing size and quality in this step, and suitable loading scenarios and boundary conditions were applied. Fatigue life prediction utilized the fatigue analysis tools in ANSYS to forecast the number of cycles to failure. based on the fatigue parameters of the material and the results of the stress study.

The goal of the research was to create a strong framework for designing infill patterns-based fatigue durability enhancement of additively built composite structures by combining these suggested approaches and models. This method not only increases structural performance but also provides useful information for upcoming production and design procedures.

1.4 The Thesis Outline

There are five chapters in this thesis. Chapter 1 outlines the goal and overall parameters of the research.

Chapter 2 presents a literature survey related to the thesis topic.

In Chapter 3 the approaches and models used to evaluate the fatigue life are described.

Chapter 4 presents the fatigue performance of different infill patterns and densities, of carbon fiber reinforced polyamide, ABS, and PLA materials.

Chapter 5 concludes the findings a thorough assessment of the variables affecting the mechanical performance of models that are 3D printed.

CHAPTER 2

LITERATURE REVIEW

2.1 Introduction to 3D Print Techniques

3D printing, also known as additive manufacturing, starts with a digital model and builds three-dimensional objects layer by layer. This technology allows for the creation of intricate and customized shapes that would be difficult or impossible to produce using traditional manufacturing methods. Nowadays, 3D printing technology impacts research and manufacturing across various industries, from small to large enterprises.

Additive manufacturing is being used more and more to produce useful end-use items as material science develops. High-performance materials, such as metal alloys and carbon-fiber-reinforced composites, make it possible to fabricate structural parts, like engine parts and interior components, that satisfy the demanding standards of the automotive industry [13]. The use of 3D printing has altered the vehicle design prototyping process. Designers may swiftly create and test different revisions of parts thanks to rapid prototyping, which speeds up development times and lowers costs. Using 3D printing technologies, companies like Ford and General Motors have achieved considerable reductions in prototype development time[14]. 3D printing makes it feasible to produce highly optimized and detailed designs that are frequently impossible to construct with conventional procedures. To create more efficient aircraft, lattice structures and topology-optimized components, for example, drastically reduce weight while retaining strength[15]. The 3D printing techniques is also applied in aerospace industry as said in [16] All facets of the aerospace sector, including military and commercial airplanes, space applications, and missile systems, are being revolutionized by additive manufacturing (AM). This change is the result of additive manufacturing's (AM) special capacity to create parts with

intricate designs, lower manufacturing costs (material waste, assembly required because of part consolidation, and tool and fixture requirements), and fabricate parts using premium materials in small batches with quick turnaround times. Additive manufacturing involves a series of steps that convert a digital model into a physical object. The process begins with creating a 3D model using Computer-Aided Design (CAD) software and then saved as a stereo-lithography file (STL) to set parameters before printing[17]. The file is then processed by slicing software, which divides the model into thin horizontal layers and generates a tool-path for the printer. Depending on the specific AM technology, appropriate materials (such as thermoplastics, photo-polymers, metals, or composites) are prepared for printing. At the printing step, the AM machine builds the object layer by layer according to the tool-path. Each layer is deposited and fused through various mechanisms, such as extrusion, laser sintering, or electron beam melting. After printing, the part may require post-processing steps such as cleaning, curing, heat treatment, or surface finishing to achieve the desired properties and quality.

2.2 Types of Additive Manufacturing Technologies

Several AM technologies exist, each with unique mechanisms and applications. The most common types include Stereolithography (SLA), Fused Deposition Modeling (FDM), and Selective Laser Sintering (SLS).

2.2.1 Stereolithography (SLA)

Stereo-lithography (SLA) is a type of 3D printing technology that falls within the vat photopolymerization category. It works by solidifying layers of liquid resin with a laser to build a three-dimensional object. Although SLA historically has been associated with creating items from a single material, advances in materials science have led to the developing of composite resins for SLA. In SLA composites, additional components are mixed with the traditional liquid resin to enhance the mechanical, thermal, or other properties of the printed item. These composites can

be used in a wider range of applications due to their properties, such as improved strength, stiffness, or heat resistance [18].

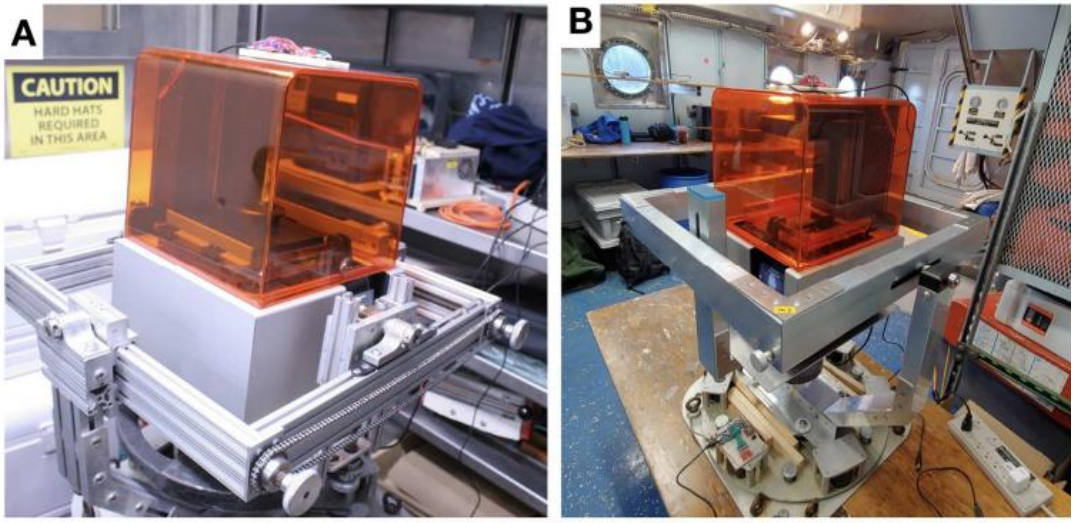

Figure 1: 3D-printer machine by SLA[19].

Xu, et al., [20] described for the first time, the use of 3D printing with stereolithography (SLA) to create new indwelling bladder devices that use an elastic polymer to distribute lidocaine hydrochloride in a localized and extended manner. The devices were intended to be used with a urethral catheter to be placed into and removed from the bladder.

2.2.2 Selective laser sintering (SLS)

SLS uses a laser to sinter powdered materials typically metals or polymers layer by layer to create three-dimensional structures. To enhance the mechanical properties of the finished printed product, reinforcing elements are typically added to the sintered polymer matrix in SLS composite [21].

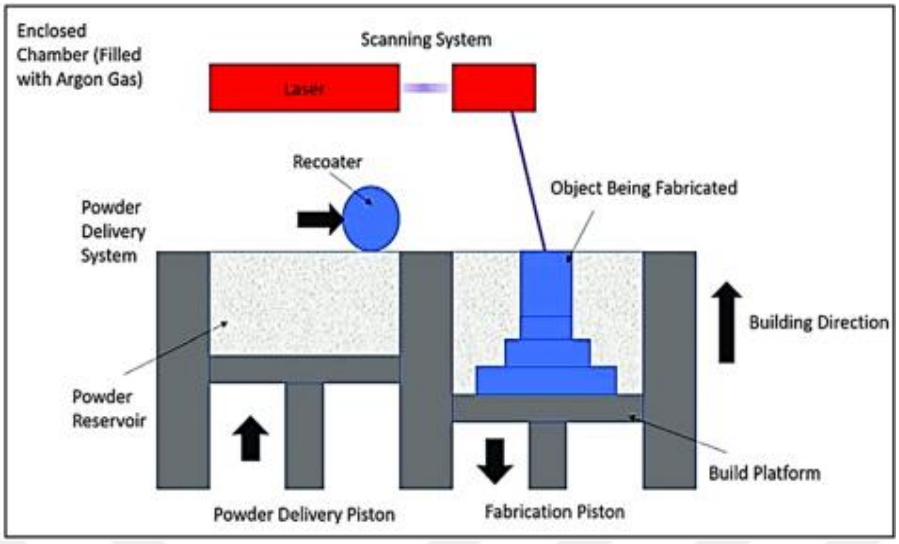

Figure 2: selective laser sintering 3D printer [22].

Even though the procedure appears straightforward, it is crucial to carefully regulate the parameters in order to prevent potential flaws such as pores, microcracks, layer delamination, warping, and degradation in the manufactured part's final property. Specifically, the secret to producing high-quality parts is accurate laser parameter control. For example, powder material right below the laser beam's center absorbs more energy than powder material below the beam's perimeter. This encourages spattering and causes an uneven melt pool to emerge [22]. For the production of polymeric components, two of the most advanced powder bed fusion additive manufacturing processes are Selective Laser Sintering (SLS) and Multi Jet Fusion (MJF). The physicochemical characterization of raw powder materials (EOS PA2200 and HP 3D HR PA12) and their printed specimens, as well as the mechanical performance and printing characteristics of printed objects, were all systematically benchmarked and compared for polyamide 12 (PA12) parts printed by SLS and MJF in this work [23].

2.2.3 Fused Decomposition Modeling (FDM)

Using a nozzle to extrude melted thermoplastic filament, fused deposition modeling also referred to as fused filament fabrication (FFF) is a 3D printing method that

builds objects layer by layer. FFF is extensively utilized in many different industries because of its affordability and adaptability. To enhance the mechanical, thermal, or other properties of printed products, FFF composites combine polymers with reinforcing fibers or particles in the filament [24].

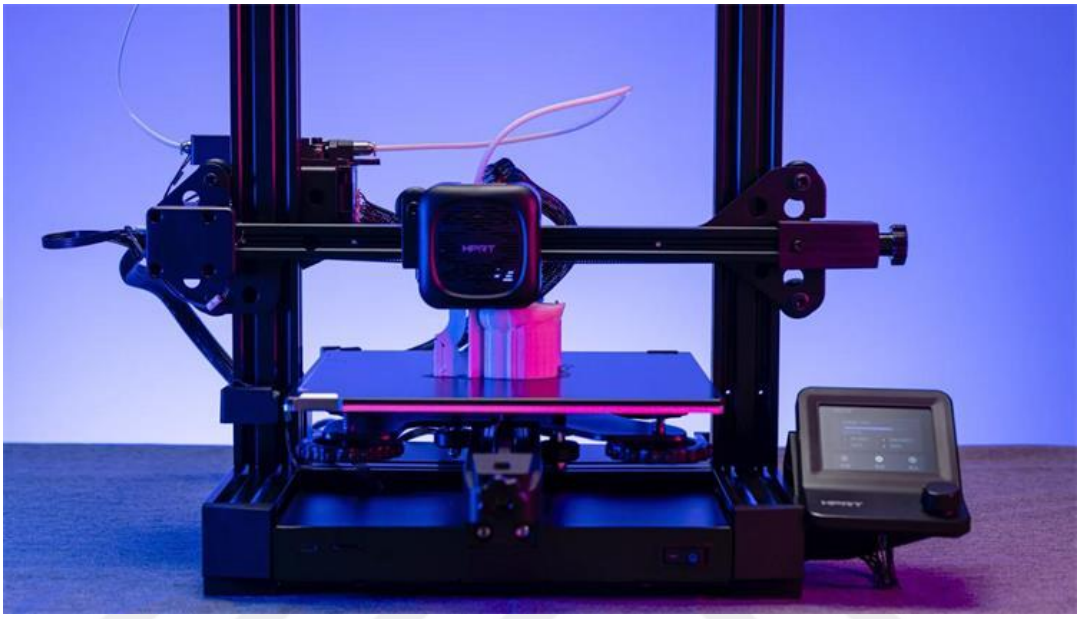

Figure 3: FDM 3D-printer machine [25].

FDM is one of the most popular additive manufacturing techniques used for a wide range of technical applications. Stratasys Inc., USA, commercially commercialized the FDM method in the early 1990s. The precise selection of process variables is the primary determinant of the quality of items produced with FDM [26]. in this study [27] the FDM process has explained as, A filament is run through a heated element during the physical process of making a model, turning it into molten or semi-molten. Using a solid filament as a piston, the liquefied filament is fed through a nozzle and deposited onto the partially formed item. Adjacent previously deposited material fused with freshly deposited material. In accordance with the geometry of the layer that is currently being printed, the head travels in the X-Y plane and deposits material. The platform that is holding the part travels vertically in the Z direction to start depositing a fresh layer on top of the one that has just been completed. The head will have deposited a complete physical representation of the original CAD file after a certain amount of time, which varies according on the volume of printed part. There is no need

for hardening because the model is finished. A second nozzle in the head of the production machine is used to extrude support material. This is in charge of providing building support for any structure that, by default, has an overhang angle less than 45 degrees from the horizontal. Support materials are disintegrable or dissolveable. With the use of 3D printing, pediatric medication dosage individualization can be achieved, bringing the precision medicine concept to reality [28].

2.3 Reinforced and Non-Reinforced Polymers for FDM Printing

The choice of polymer material in FDM significantly impacts the mechanical properties, durability, and applications of printed items. The two primary types of polymers used in FDM are reinforced and non-reinforced.

2.3.1 Reinforced Polymers

To improve the mechanical and physical properties of the base polymer, filaments or beads are added as reinforcements. These reinforcements significantly improve the strength, stiffness, and sometimes the chemical and heat resistance of the printed parts. (To improve the strength and stiffness of the material, carbon fibers are incorporated into the underlying polymer such as PLA, ABS, or Nylon [29, 30]. low weight and superior strength-to-weight ratio make these reinforced thermoplastics suitable for high performance and useful in a variety of industries, including the automotive, aerospace, and medical sectors. Glass fibers are added to base polymers to increase their strength and durability, are utilized in applications where slight increases in strength are adequate and are often less expensive than carbon fiber composite. Kevlar fibers are used in applications where high toughness and durability are required due to their exceptional impact resistance. Metal Powder Reinforced Polymers combine a polymer with metal particles like copper, bronze, or stainless steel are used to improve strength, resistance to wear, and thermal conductivity. These composites may also have special visual qualities, including a metallic sheen.

The most significant kind of composites are thought to be fiber-reinforced composites. High strength, stiffness, and resistance to temperature, chemicals, and wear are among the improved material properties displayed by dispersed phases of natural or synthetic fibers, such as glass, carbon, basalt, and aramid, in a composite structure. Primarily, the goal of creating fiber-reinforced composites is to have high moduli and specified strengths. The fibers can be aligned or randomly oriented based on the array in the composites, or continuous or discontinuous depending on the fiber's length) [30].

Particle-reinforced composites may be 3D printed with the material's characteristics customized for particular uses. The examination of the hardness changes with the volume percentage of the hard particle in the particle-reinforced composite has been done using many models for a rule of mixtures and the finite element approach. It is found that for large hard particle volume fractions, the stress states are almost iso-strain, while at low particle volume fractions, they are iso-stress [31].

Metal matrix composites provide considerably improved features such as better strength, stiffness, and weight savings [32]. The cost-effectiveness, isotropic qualities, and processing compatibility of particle-reinforced MMCs make them appealing compared to monolithic materials.

In particle-reinforced composite materials, the distribution, shape, size, and orientation of the reinforcing particles all play a significant role in the development of cracks. Therefore, it is crucial to include the intricate micro structure of the particles and not only approximate it using circles or ellipses to effectively predict fracture formation in such a system. This paper has used the finite element approach to study the impact of particle morphology and distribution (homogeneous and clustered) on crack formation [33].

2.3.2 Non-Reinforced Polymers

The base materials used in FDM printing are non-reinforced polymers, sometimes referred to as pure or unfilled polymers These are usually thermoplastics, which are

perfect for the layer-by-layer deposition process in FDM since they soften when heated and solidify when cooled. Typical non-reinforced polymers for FDM consist of polylactic acid, or PLA, which is a biodegradable, easily printable substance with a low warp and a smooth surface. It's well-liked for instructional and prototyping uses.

Acrylonitrile butadiene styrene, or ABS, is well-known for its sturdiness, resilience to impact, and strength. It is frequently used for functioning pieces and necessitates a heated bed to prevent warping. Polyethylene terephthalate glycol, or PETG, strikes a fair compromise between PLA's ease of use and ABS strength. It resists chemicals well and is robust and long-lasting. Nylon is well-known for having exceptional mechanical qualities, including as great flexibility and tensile strength. it is applied to parts that need to be resistant to wear and tear [34].

In terms of printability, printing non-reinforced polymers is simpler and involves fewer problems with print bed adherence and nozzle wear. Hardened steel or ruby nozzles may be necessary for reinforced polymers since they can quickly wear out nozzles, particularly when the polymers contain abrasive fibers like carbon or glass.

However, industrial applications, functional parts, and situations needing improved mechanical qualities, reinforced polymers are the recommended choice. In conclusion, the decision between reinforced and non-reinforced polymers in FDM printing is based on the particular needs of the application, taking into account cost, printing ease, strength, and durability.

2.4 FDM Process Parameters

FDM is a widely used additive manufacturing technology that is highly regarded for its ability to produce complex structures utilizing a variety of thermoplastic materials) [17]. Several critical process variables affect the final product's strength, quality, and accuracy. Comprehending and refining these factors is essential to attaining the intended outcomes in FDM printing. Layer height, print speed, cooling rate, infill density and pattern, print orientation, support structure, and extrusion and

bed temperatures are the FDM parameters. FDM process parameters fall under the following categories:

The parameters that are adjusted at the slicing step: air gaps (between rasters and between perimeters), the number of contours/perimeters (width of contour), top and bottom thicknesses, nozzle diameter, bead width, road width, flow rate, deposition speed, infill, raster orientation, and angle, raster pattern. Orientation based parameters: testing specimens are typically positioned laterally, vertically, or horizontally; however, alternative orientations may be employed as well; temperature conditions include bed or platform temperature, intrusion temperature, and ambient (or envelope) temperature.

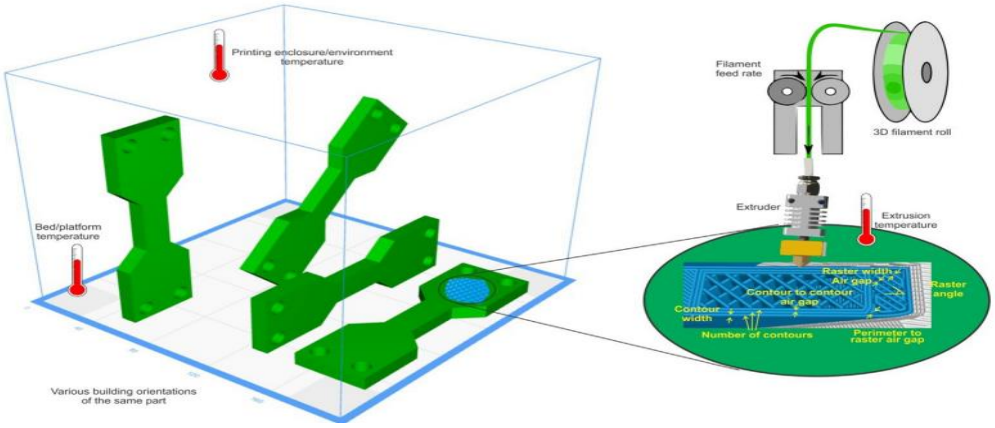

Figure 4: FDM process parameters illustration [35].

Popescu, D., et al [35], achieving optimal FDM process settings necessitates balancing print speed, quality, strength, and material consumption. They found that each parameter affects the others, therefore a thorough grasp of how they interact is necessary. Among the difficulties are material-specific adjustment, complex geometries, and consistency. Recognizing the valuable and practical elements, important process variables, and constraints, as well as determining the degree to which the findings of these studies are pertinent and applicable to future research and practical applications.

In [36] a thorough literature search was conducted using a classification system based on the kind of polymer used in 3D printing, the most important process variables that are thought to affect the tensile, compression, flexural, or impact

strengths of FDM specimens are examined in light of the findings reported in the literature.

In [37] the relationship between printing orientation, internal structure, and the tensile characteristics of 3D-printed short fiber reinforced composites was investigated.

In [38] the universal testing equipment was used to observe the tensile properties through fracturing development and material failure. The specimen was able to withstand a tensile force of 31.69 MPa. The specimen's maximum yield strength was higher regardless of the infill structure. Similarly, reducing the specimen's yield strength deviation meant increasing the infill ratio.

In [38] found that the specimen fractured as a result of linkages in the infill structures breaking. Based on the observations, the high bonding area of the hexagonal infill structure contributes to its good tensile performance.

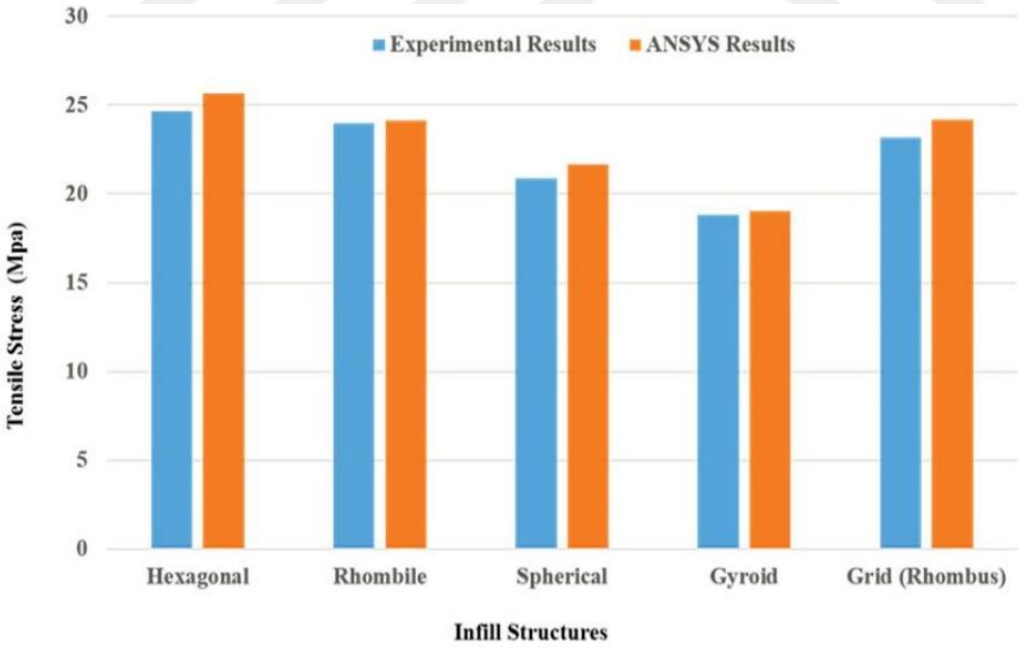

Figure 5: tensile stress with for various infill structures [38].

This demonstrates the yield stress similarity seen in the honeycomb, a hexagonal infill construction with an ultimate tensile strength of 13.79 MPa. It was discovered

that the hexagonal infill structure had good tensile performance when compared to other infills. All infill constructions exhibit a pattern of increasing yield strength in direct proportion to the weight of the added material. Because of the infill material's bonding strength, spherical and gyroid infill structures have lower tensile values. When compared to the honeycomb structures, the infill's patterns' area of contact is less [38].

2.5 Fatigue life of 3D-Print Composite

the amount of stress and strain cycles or repetitions that a material can bear before failing is referred to as the fatigue life [39].

In [40], the performance of two non-woven AM printed composites (unidirectional and multi-directional fibers), a woven composite, and a composite reinforced with chopped carbon fibers were compared using tensile, flexural, and fatigue testing.

Figure 6: fracture modes observed during tensile testing[40].

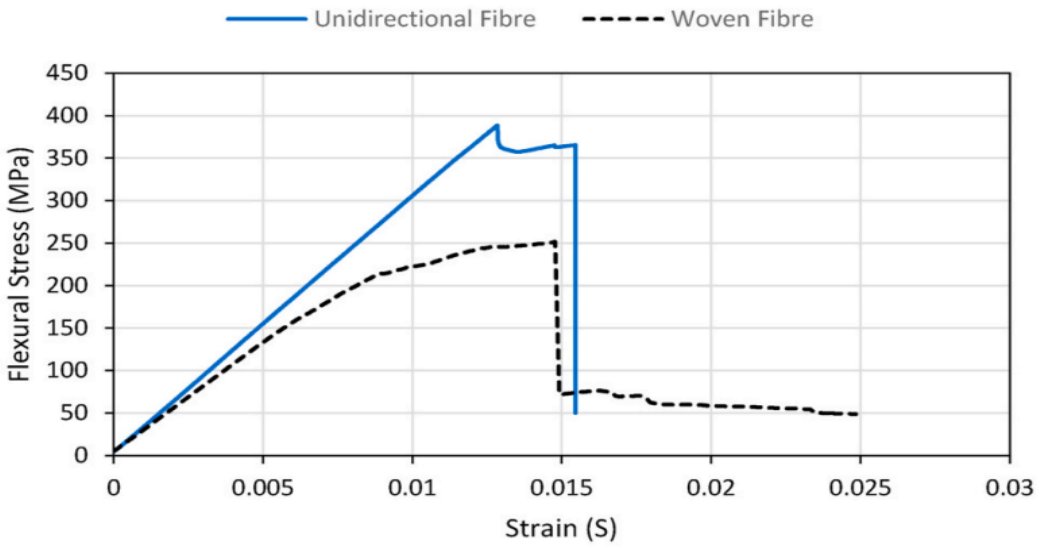

Figure 7: atypical stress-strain curve of unidirectional and woven carbon fiber [40].

In [40] investigated the mechanical properties of short fiber reinforced composites created using fused deposition modeling rely on a number of variables, such as the internal structure of the material and printing properties.

ANSYS was used to simulate the fracture evolution of the ASTM D 638 specimen. The graphic displays the stages of development. Stress builds up at the weaker areas of the specimen as a result of mechanical stress applied to one end of the specimen. The interior layers of the infill receive the tensile load instead of the outer layers. Because the specimen is oriented at a zero-degree angle, the infill's bonding is perpendicular to the direction of the applied tensile force [38].

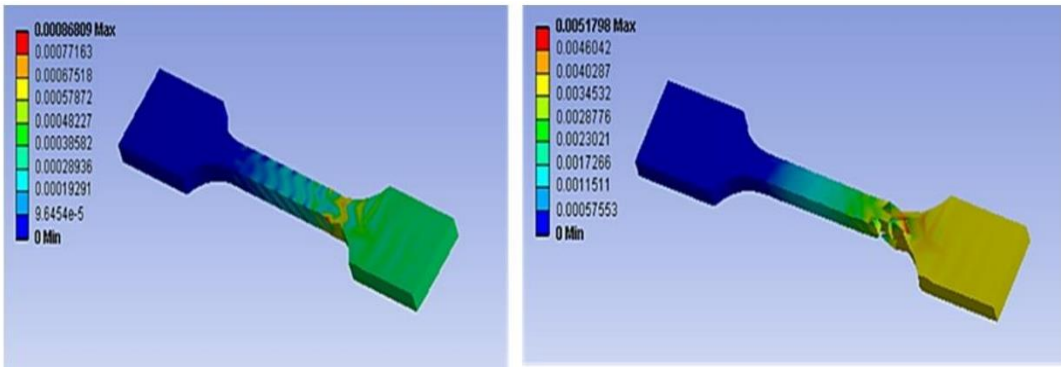

Figure 8: finite element results[38].

In [38] the specimen fractured as a result of linkages in the infill structures breaking. Based on the observations, the high bonding area of the hexagonal infill structure contributes to its good tensile performance.

FDM printed parts often have lesser strength and fatigue life when compared to those made using alternative manufacturing techniquesTo overcome this limitation, researchers have investigated the use of fibers and reinforcements to enhance the mechanical properties of FDM products. On the other hand, a variety of production parameters may significantly affect how well FEM-produced parts work [12]. One such parameter is infill density, which is crucial for striking a balance between cost and time. By adjusting the infill density (50 and 75%) and raster angle (0°, 45°, and 90°), the tensile strength and fatigue life of carbon fiber-reinforced poly-lactic acid (PLA) composites made by FDM were examined in [12] .

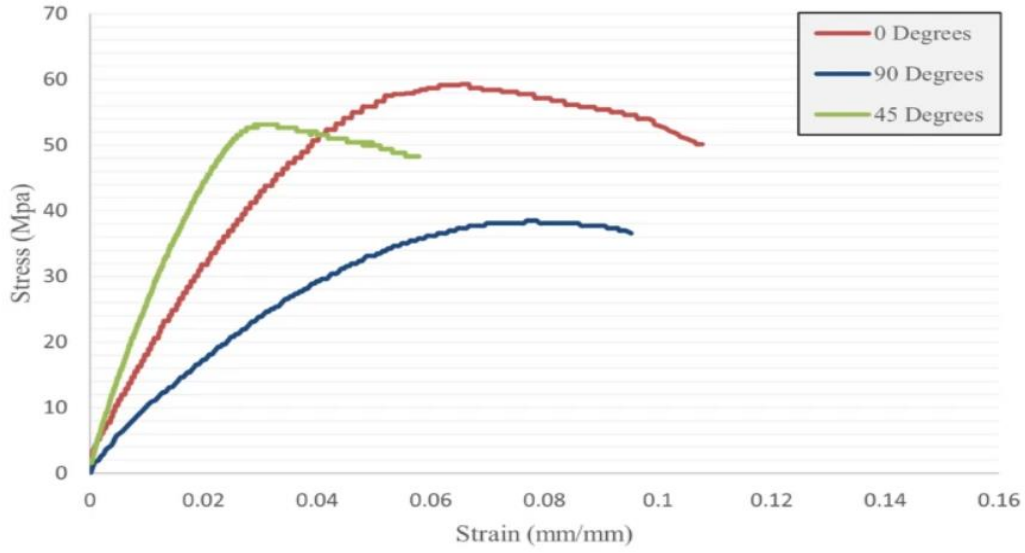

Figure 9: Stress-strain curve of carbon fibers reinforced PLA [12]

Figure 9, shows a stress-strain curve for a material evaluated at three distinct orientations 0, 45, and 90 degrees. The orientation with the highest stress values, or 0 degrees (Red Curve), indicates that the material can withstand the greatest force before failing. Around 65 MPa is the ultimate tensile stress, and the curve shows a considerable amount of plastic deformation before collapse. The ultimate stress in 45 degrees (Green Curve) orientation is moderate and is around 55 MPa. Though not

as much as in a 0-degree position, the material does exhibit some plastic deformation. The direction with the lowest peak stress, around 35 MPa, is 90 degrees (Blue Curve). Comparing this orientation to the other two, the material fails at a lower strain and shows less plastic deformation. One of the main issues with FFF components is the anisotropy of mechanical characteristics brought on by part-build orientation and raster orientation [41].

In [41] investigated the anisotropy of PETG coupons by contrasting them with four distinct raster orientations: diagonal, transversal, longitudinal, and crosshatched.

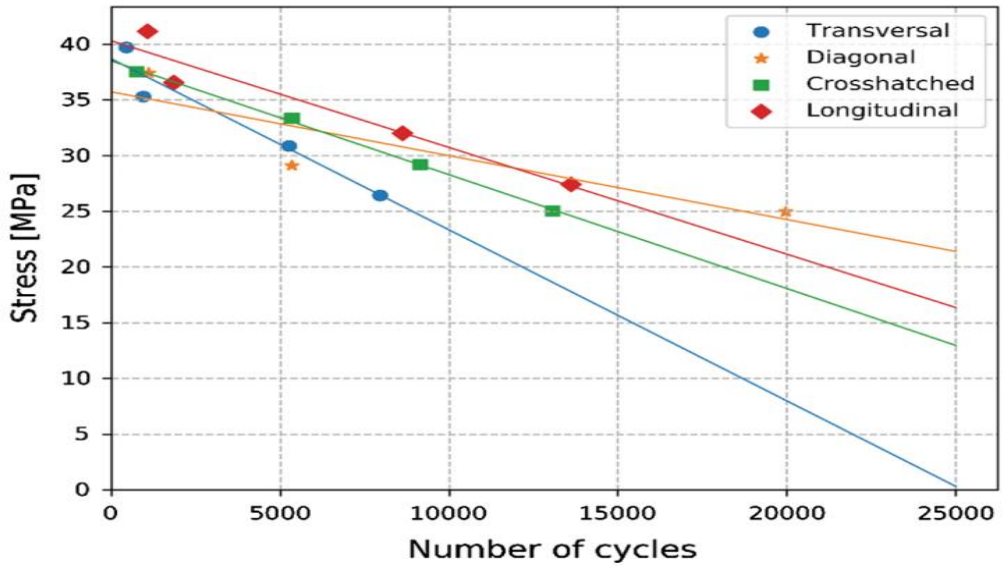

Figure 10: S-N curves for samples oriented differently [41].

Accordingly. Specimens were examined at 90, 80, 70, and 60% of nominal UTS. Even though a logarithmic-scale representation of S–N curves is typically used for fatigue information, in [41] did not use the log scale due to tiny fluctuations in applied stress and a limited number of cycles before failure. Except for samples with a diagonal raster, all sample types using this representation agreed well with the linear regression curve, suggesting that the number of cycles was proportionate to the fatigue deterioration.

2.6 Additive Manufacturing Optimization

In [42] had overview on the problems and prospects for using topology optimization techniques in AM. The primary analysis concerns addressed are how to reach the highest geometric resolution possible so that the optimization model can include the fine characteristics that AM can easily produce.

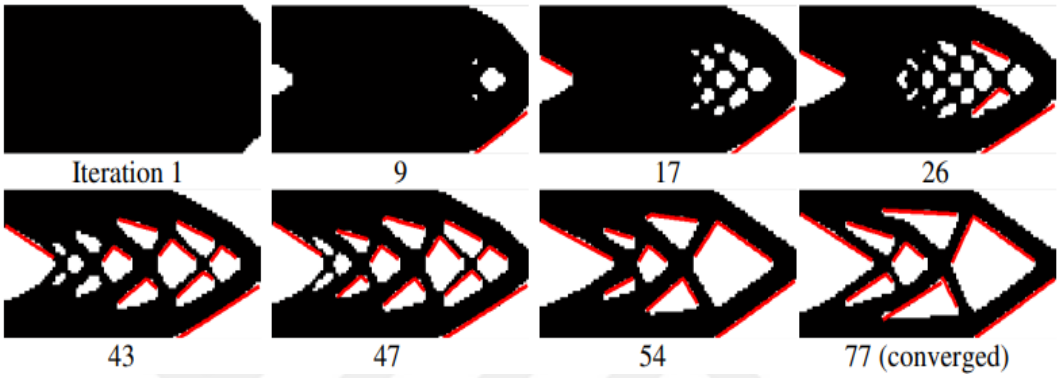

Figure 11: Iterative downward facing edge analysis during topology optimization[42]

In [43] topology optimization is a sophisticated structural design process that was created to produce high-performance, lightweight combinations that are hard to achieve with traditional principles. With the use of layer-by-layer connecting material, additive manufacturing is an advanced manufacturing technology that creates structures exactly as intended while offering a different pattern for intricate components.

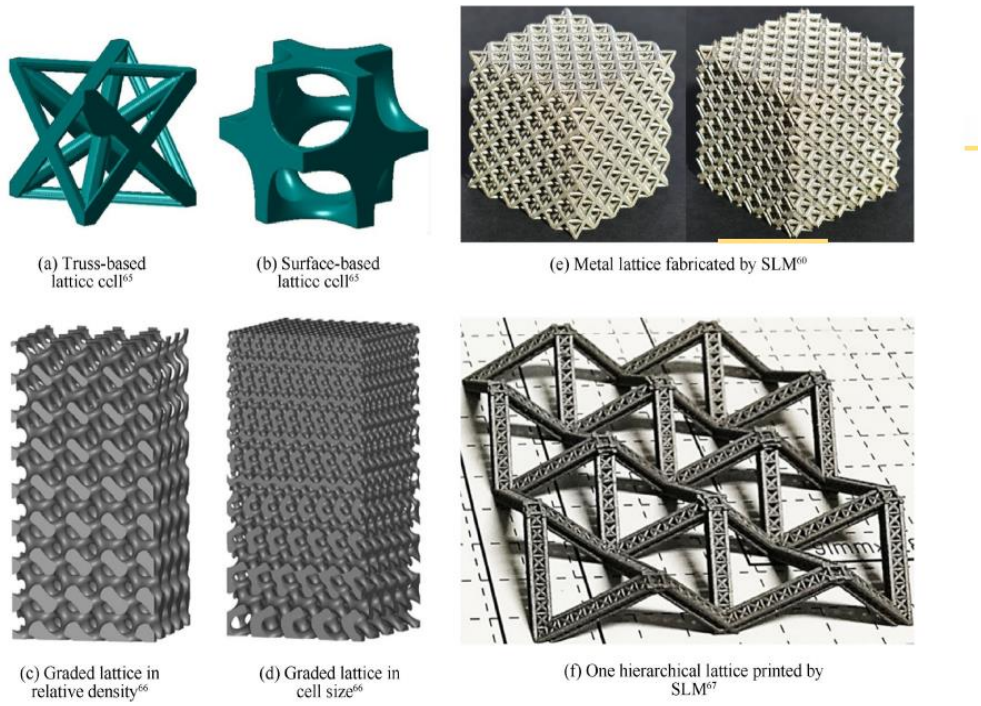

Figure 12: lattice example[43].

In [43] although graded and scaled lattice solutions can significantly enhance mechanical performance when compared to a uniform lattice structure, lattice solutions still perform worse mechanically than solid solutions. Each strut is used as the fundamental unit in the numerical analysis process for truss-based lattice structures, while the lattice unit cell simply acts as an auxiliary modeling tool. Graded hierarchical structures are obtained by implementing strut-sizing optimization [43].

In [44] in the last 20 years, there has been extensive research on manufacturing-oriented topology optimization, particularly focusing on traditional production methods such as machining, injection molding, and casting. These initiatives have provided almost ideal and easy-to-manufacture design solutions, benefiting both design and manufacturing engineers. Recently, there has been a strong focus on additive manufacturing by both industry and academic.

a Solution with minimum self-supporting angle of 26.6 degrees, $f = 109.53$, $f_{\eta=0} = 103.42$.

b Solution with minimum self-supporting angle of 45 degrees,, $f = 116.11$, $f_{\eta=0} = 108.38$.

c Solution with minimum self-supporting angle of 63.4 degrees,, $f = 174.69$, $f_{\eta=0} = 158.95$.

Figure 13: Using a 3D Systems Pro-X 300, topology optimization was performed for a self-supporting 45-degree overhang in 17-4PH stainless steel [44].

In [44] The outcomes of additive topology optimization for a structural design under various restrictions for the minimal self-supporting angle are displayed in the Figure 13. The three sub-figures (a, b, and c) show several optimization solutions with different angles of self-support.

CHAPTER 3

FINITE ELEMENT SIMULATION

3.1 Process Parameters for Fatigue Investigation

In the scope of this study, fatigue investigation was performed using the stress-life method by applying constant amplitude loading. A typical instance of constant amplitude loading between a minimum and maximum stress is depicted in Figure 14 Minimum stress (σmin), maximum stress (σmax), mean stress (σm), alternating stress, or stress amplitude (σa), and stress ratio (R) are the characteristics of the constant amplitude stress scenario. The following relations are evident in Figure 14:

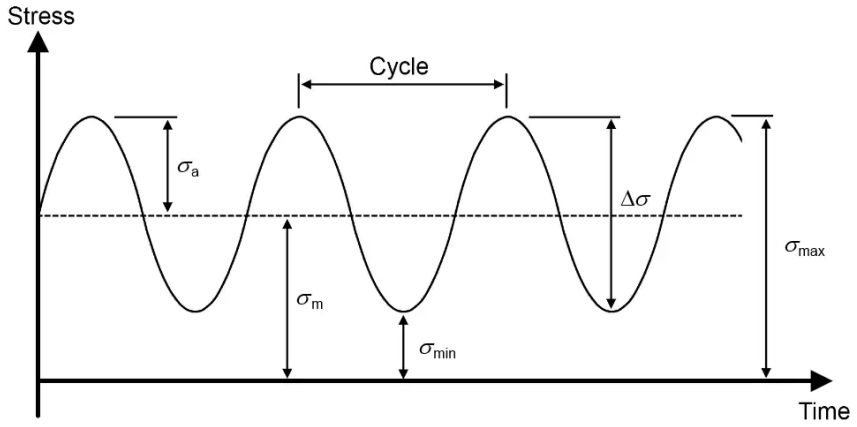

Figure 14: general constant amplitude loading

$$\sigma_m = \frac{\sigma_{max} + \sigma_{min}}{2} \tag{3.1}$$

$$\sigma_a = \left|\frac{\sigma_{max} + \sigma_{min}}{2}\right| \tag{3.2}$$

$$R = \frac{\sigma_{min}}{\sigma_{max}} \tag{3.3}$$

3.2 Infill Modelling

Solid Works was used to design the models, including infilling patterns and infill densities.

Infill patterns refer to the geometric shapes used to fill the interior of a 3D-printed object. while Infilling density refers to the percentage of the interior volume of a 3D-printed object filled with material. Figure 15, Figure 16, and Figure 17 present a honeycomb, rectilinear, triangle, and infilling densities of 25%, 50%, and 90%. The models were designed in Solid-works to right weight, saving material, and printing time while maintaining mechanical performance.

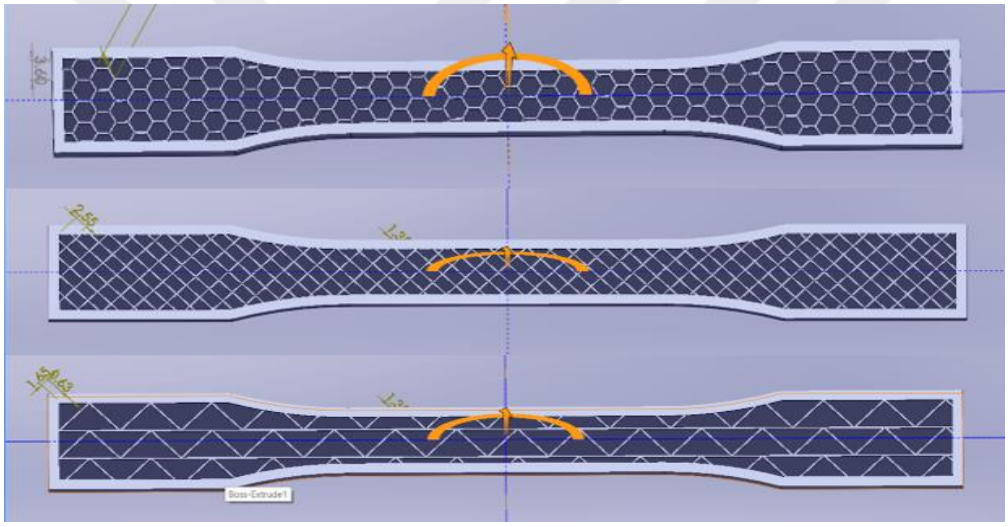

Figure 15: infill pattern honeycomb, Rectilinear, and Triangle both on 25% infill.

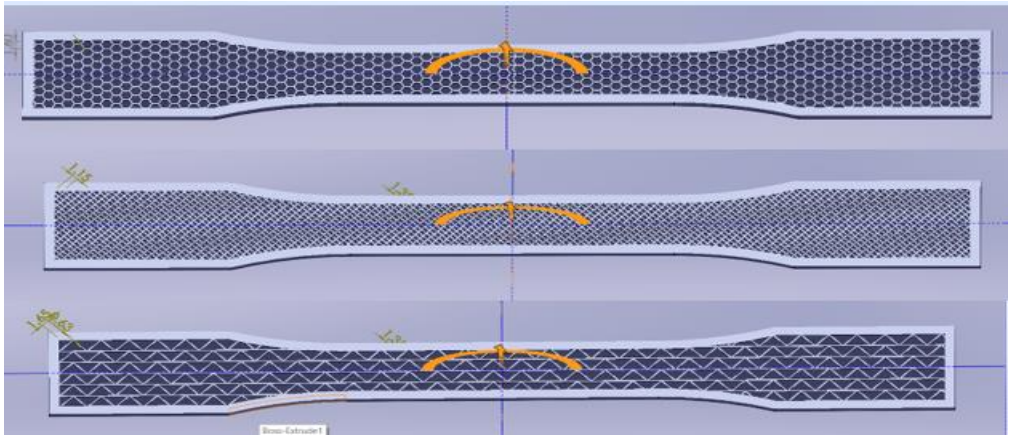

Figure 16 infill pattern Honeycomb, Rectilinear, and Triangle with 60% infill parentage

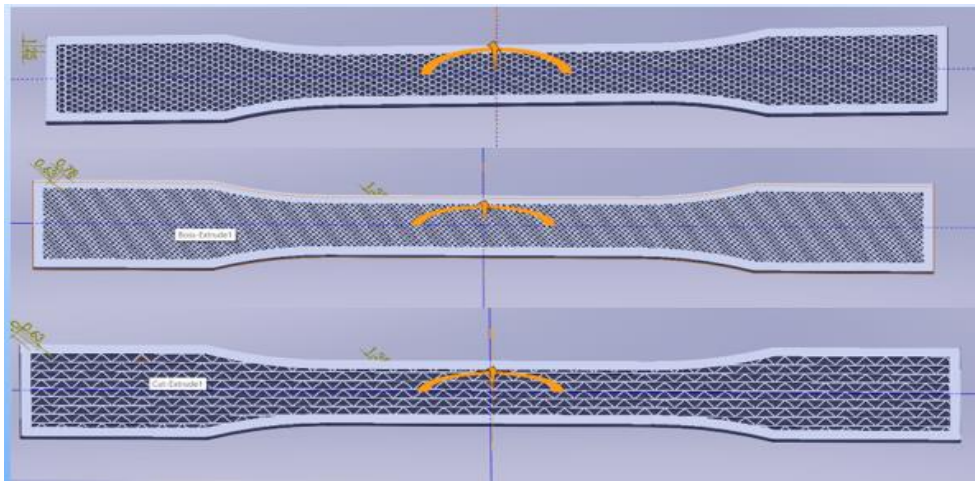

Figure 17: Infill honeycomb, Rectilinear, and Triangle with 95% infill density.

3.3 ANSY Fatigue Simulation

Using ANSYS software, we performed a numerical analysis to precisely examine fatigue behavior. In this investigation, the stress-life technique was utilized to mimic the fatigue behavior of finite elements. With this technique, the sample is subjected to an oscillating stress, and the number of cycles measured until failure represents the sample's life. The loading ratio was taken into consideration in the analysis at 0.1. The software integrated the mechanical and physical characteristics of PLA, ABS, and PA12CF into its materials database.

Table 1 outlines the physical and mechanical properties of ABS, PLA, and PA12CF. Also, the S-N data for ABS, and PLA material was extracted from the literature while PA12CF S-N curve, ultimate tensile strengths, and yield strength were tested in lab, while young' s modulus were calculated from Halpin-Tsai formula. Data were tabulated in Table 2.

Table 1: Material properties of the filaments

	Material		
Properties	ABS[45]	PLA[46]	PA12CF
Density (gr/cm^3)	1.15	1.25	1.11
Young's modulus (MPa)	1282	3600	33972
Poison, 's ratio	0.3	0.3	0.28
Tensile yield strength (MPa)	15.3	58	26
Ultimate yield strength (MPa)	16.9	64	40.2

Table 2: S-N data for the material

ABS[45]		PLA[46]		PA12CF	
Stress (MPa)	Cycles	Stress (MPa)	Cycles	Stress (MPa)	Cycles
15.21	1155	50	65	30	819
12.75	4593	48	95	20	45719
10.15	13628	42	450		
8.45	24000	40	750		
		38	1000		
		35	2800		
		32	5000		
		30	6500		
		28	10000		
		25	28000		
		20	55000		
		15	100000		
		10	1000000		

3.4 Determining the Mechanical Properties of Carbon Fiber-Reinforced Polyamide PA12CF

To calculate longitudinal Young's modulus, the E_1 semi-empirical Halpin-Tsai model was used [47]:

$$\frac{E_1}{E_m} = \frac{1 + \xi\eta v_f}{1 - \eta v_f} \tag{3.4}$$

Where η is given by

$$\eta = \frac{E_f/E_m - 1}{E_f/E_m + \xi} \tag{3.5}$$

$$\xi = \frac{2L}{d} \tag{3.6}$$

Where E_f and E_m are the modulus of elasticity of the fiber and matrix respectively, L is the length, and d is the diameter of the fibers.

Thermogravimetric analysis (TGA) was used in the nitrogen atmosphere to measure the weight (w_f) and the fiber volume fraction (V_f) of the embedded short carbon fibers. The temperature range covered by TGA was 25 °C to 400 °C with a 10 °C/min increase Considering the densities of each component in the filament (ρ_m, ρ_f) and the volumes of matrix and fiber (v_m, v_f) are determined using Equation 4a and Equation 4b [37].Then, the fiber volume fraction is determined through Equation 5 [37].

$$v_m = \frac{w_m}{\rho_m} \tag{3.4a}$$

$$v_f = \frac{w_f}{\rho_f} \tag{3.4b}$$

$$V_f = \frac{v_f}{v_m + v_f} \tag{3.7}$$

The study revealed that the carbon fibers had a weight ratio of 13%. The carbon fibers' density is $\rho_f = 1.15$ g/cm^{3}and the matrix material's is $\rho_m = 1.13$ g/cm^3, respectively, for the component materials. Using these data, the fiber volume ratio is computed as $V_f = 0.14$.

Scanning electron microscopy was used to measure the diameter and length of the inserted carbon fiber (SEM). The glass fibers were measured to have an average diameter of 10 μm and an average length of 300 μm.

Transverses Young's modulus (E_2) is calculated using equation 6:

$$E_{22} = \frac{E_m}{1-\sqrt{V_f}} \cdot \frac{1}{(1-\frac{E_m}{E_f^{22}})} \tag{3.8}$$

In-plane shear modulus was calculated using Chamis's equations as presented in Equation 11.

$$G_{12} = \frac{G_m}{1-\sqrt{V^f}\left(1-{G_m}/{G_f^{12}}\right)} \tag{3.9}$$

The major poison's ratio was calculated using hamis equation.

$$\nu_{12} = V^f \nu_{12}^f + V^m \nu^m \tag{3.10}$$

Table 3: Material properties. subscript denotes the matrix, and subscript denotes the fibers.

Material property	Value	Reference
$\boldsymbol{E_m}$	12000 MPa	[48]
$\boldsymbol{G_m}$	4318.15 MPa	Study outcome
$\boldsymbol{\nu_m}$	0.89	Study outcome
$\boldsymbol{\rho_m}$	0.13	[37]
$\boldsymbol{E_f}$	276000 MPa	[48]
$\boldsymbol{E_f^{22}}$	3000 MPa	[37]
$\boldsymbol{\nu_f}$	45 MPa	[37]
$\boldsymbol{G_f}$	1.13 g/cm^3	[37]
$\boldsymbol{\rho_f}$	1.11 g/cm^3	[49]
$\boldsymbol{d}$ (avg. fiber diameter)	10 μm	Study outcome
$\boldsymbol{L}$ (avg. fiber length)	300 μm	Study outcome
$\boldsymbol{V_f}$	0.14	Study outcome
$\mathbf{V_{m12}}$	0.28	[48]

Table 4: Material properties and their values

Properties	Values
E_1	33972(MPa)
E_2	18766(MPa)
G_{12}	6354.44(MPa)
ϑ_{12}	0.286

3.5 Tensile Test

Tensile tests were conducted on the dog bone shape samples according to ASTM D639. The samples were printed on E2CF 3D printing machine using PA12CF material with 100% infill density at 00, with the aim of directly determining the ultimate tensile strength. The fatigue tests were then performed considering the observed UTS. Tensile tests were performed using the TENSON universal tensile test machine at the University of Turkish Aeronautical Association, in displacement control model at rate of mm/min.

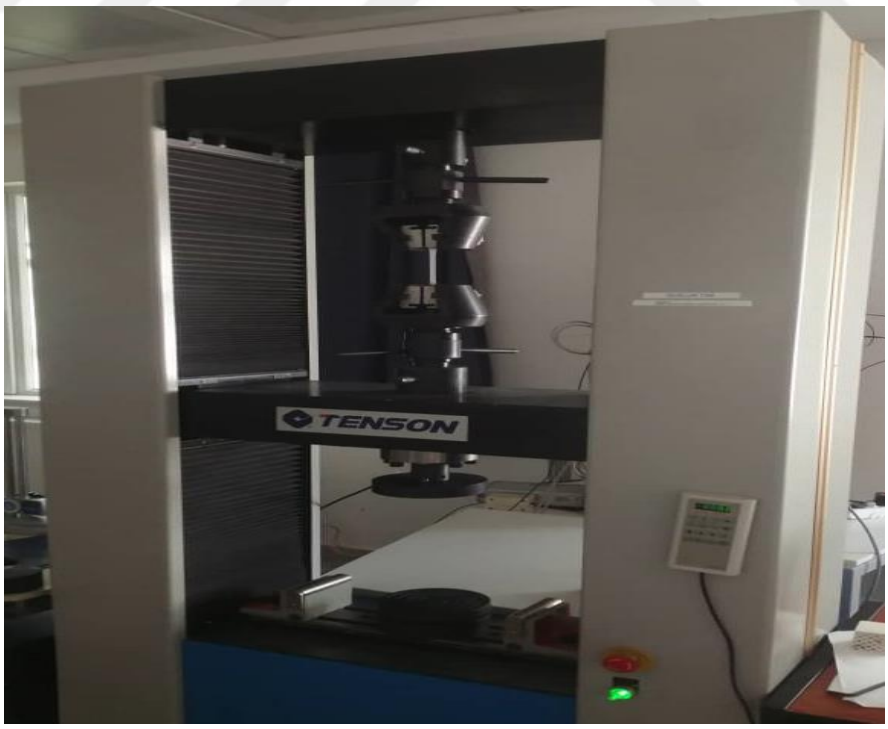

Figure 18: tensile test machine

Figure 19: 100% full solid specimen after test

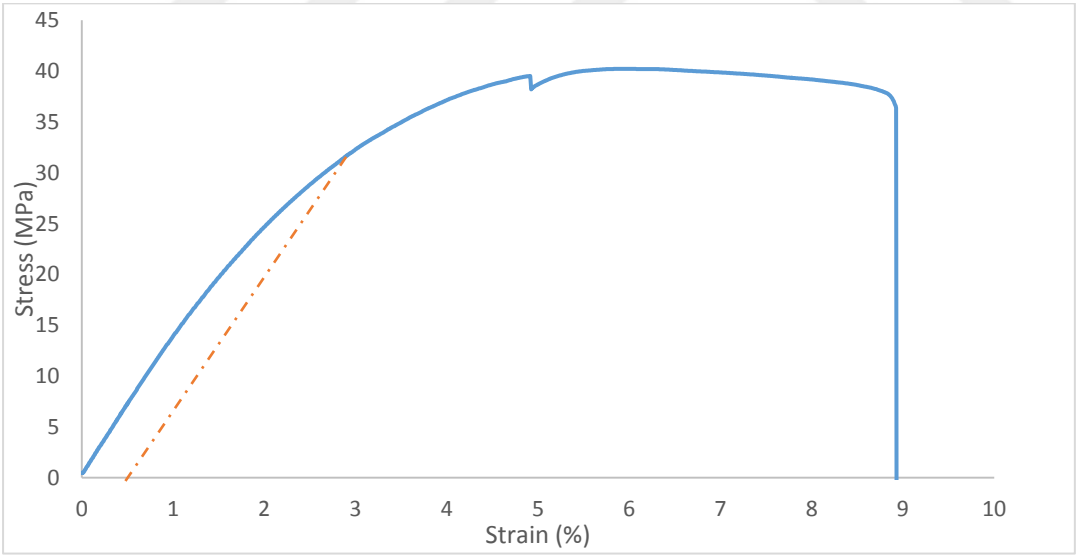

Figure 20: Shows a fractured tensile test specimen

The stress-strain curve from a tensile test on a PA12CF (Poly-amide 12 Carbon Fiber) material specimen is shown in Figure 19. There is a linear relationship between stress and strain in the first portion of the curve, up to roughly 0.2% strain. This area demonstrates the material's elastic behavior, where it deforms but then

returns to its original shape when the load was removed. The material's yield strength, or the point at which deformation changes from elastic to plastic, is shown by this point (40.2MPa). At about 5% strain, the curve reaches its maximum stress value at 40.2 MPa. The ultimate tensile strength, or the highest stress the material can bear before necking starts, is shown by this peak. The specimen eventually breaks at about 9% strain, even though the stress reduces while the strain increases.

3.6 Fatigue Simulation

The modeled parts at Solid Works were imported into Ansys software. Figure 22 displays the application of loading and support conditions. Two ends, the left end presents fixed support while the right side is the load applied.

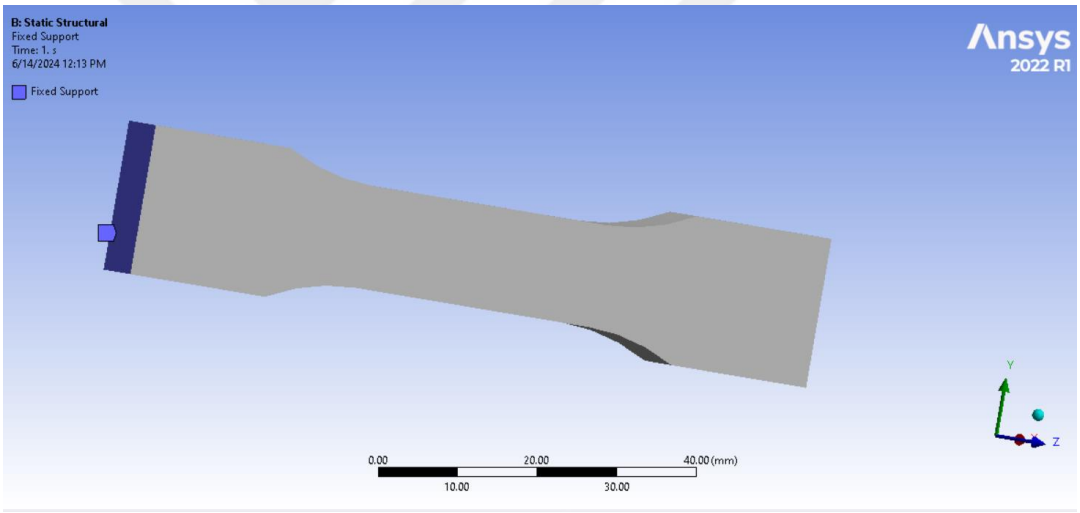

Figure 21: loading condition

For each case, the size, shape, and total number of meshes are presented in Figure 22.

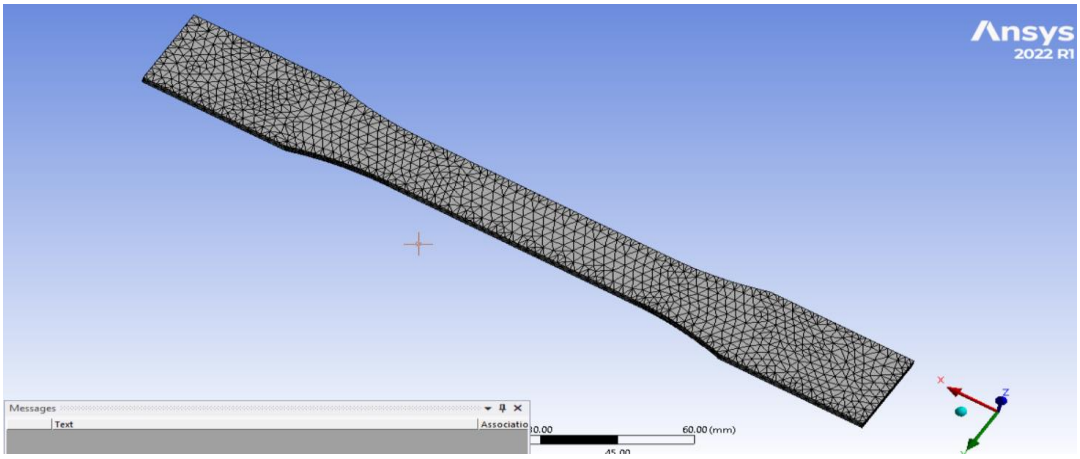

Figure 22: Boundary conditions

Table 5 presents meshing parameters including mesh type, mesh size, and mesh number.

Table 5: Mesh type, size, and total amount of mesh for various infill densities and shapes

Infill shape	Infill density (%)	Shape of mesh	Size of mesh	Number of mesh
H	25	Tetrahedral mesh	0.5mm	49042
R	25			58279
T	25			27847
H	60	Tetrahedral mesh	0.5mm	72653
R	60			171825
T	60			45148
H	95	Tetrahedral mesh	0.5mm	160600
R	95			251035
T	95			76888

In the scope of this study, the stress life method was used to predict the fatigue life. The obtained results were then used to determine Basquin's model parameters. Basquin's formula was applied due to its accuracy also used in similar works in literature [50].

$$S = A.N^{b} \qquad (3.11)$$

Where S is the tensile stress, N_f is the number of cycles to failure, A and b are material constants that represent the ultimate static stress and the dynamic hardening modulus, respectively.

The fatigue analysis was done in ANSYS where was R=0.1, as shown in equation 2.3.

MAX STRRESS= AVG SRESS*ULT TENSILE STRESS*INFILL%.

MIN STRRESS= RATIO*MAX STRESS.

1mm was set as fatigue safety factor, constant amplitude load was set to good man.

The safety factor property was to show the relationship between the applied stress and the material's strength. A more dependable design was implied by a greater safety factor. It took into consideration probable component faults, loading circumstances, and uncertainties in material qualities. This guarantees the design's safety in the event of unforeseen circumstances. Higher safety factors in fatigue analysis suggest that the component was functioning effectively within its strength limitations, which could result in longer fatigue life. This lowers the possibility of an unexpected cyclic loading condition causing an abrupt failure.

CHAPTER 4

RESULTS

This work examined how infill density and pattern affected the fatigue characteristics of materials printed with acrylonitrile butadiene styrene (ABS), poly-lactic acid (PLA), and carbon fiber reinforcedpoly-amide PA12CF.

The results showed that the infilling patterns and infilling densities have a significant impact on the fatigue life of the printed part. Table 6 presents data taken from ANSYS after fatigue analysis and then placed into Excel to investigate which filling patterns or densities have better fatigue life.

4.1 Comparison Among Infills Patterns With ABS Material

Table 6: 25 filling percentages with different filling patterns

Material	UTS	Infill density	Infill pattern	Stress	Life	Stress/uts
ABS	16.9	25%	Honeycomb	3.5	3013.3	0.2071006
				3	14413	0.1775148
				2.5	1.00E+06	0.147929
			Rectilinear	3.5	1.80E+03	0.2071006
				3	1.05E+04	0.1775148
				2	1.00E+06	0.11834319
			Triangle	3.5	4.27E+03	0.2071006
				3	3.60E+04	0.1775148
				2.6	1.00E+06	0.1538462

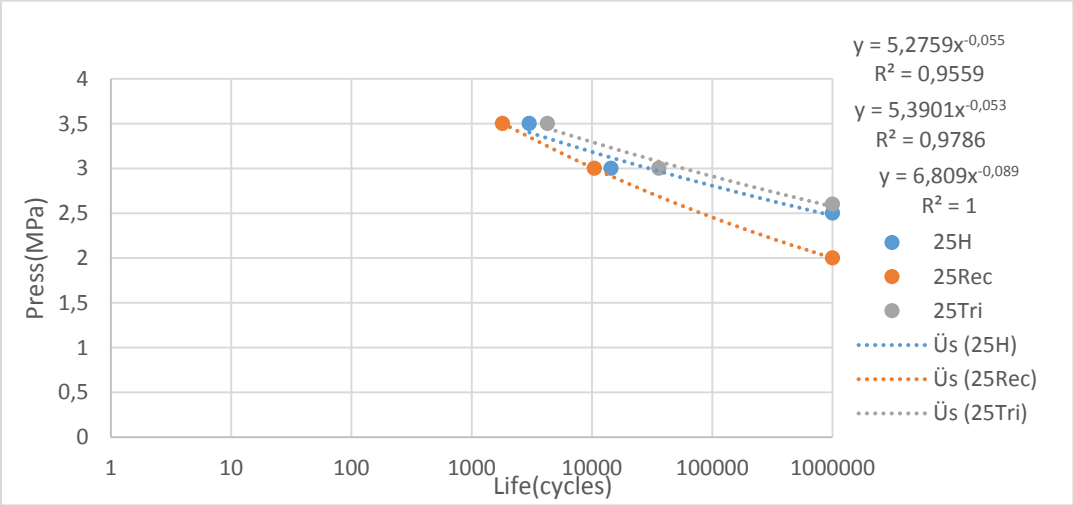

Figure 23: 25% infill density (ABS).

Table 7: 25 infill density with honeycomb, rectilinear, and triangle infill patterns (ABS)

Infill pattern	A	B	R^2
Honeycomb 25%	5.2759	-0.055	0.9502
Rectilinear 25%	5.3901	-0.053	0.9786
Triangle 25%	6.809	-0.089	1

Table 7 escribes the basquin's formula. So, the compression was made using this formula.

$$S = A.N_f^b$$

From this formula above, fatigue tensile stress is represented by S, cycles to failure are represented by NF, and ultimate static stress and dynamic hardening modulus are represented by material constants A and B, respectively.

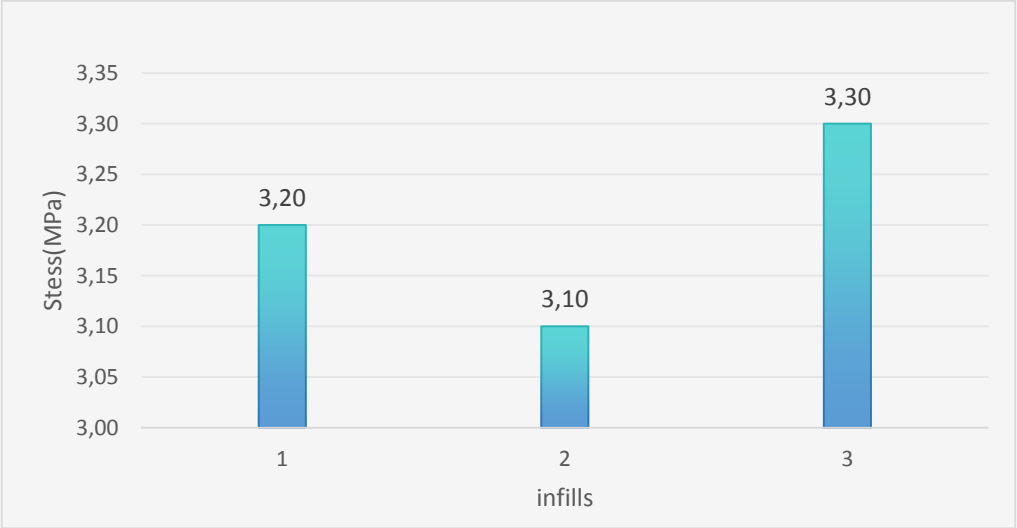

Figure 24: comparison among Honeycomb, Rectilinear, and Triangle to constant infill density of 25% ABS

Figure 24 shows the fatigue behavior for three distinct infill patterns (hexagonal, rectangular, and triangular) printed under a 25% filling density model. 1 presents honeycomb, 2 presents rectilinear, and 3 presents triangle. The comparison was done using Basquin's formula where data are displayed in Table 7 A, B, and N. The number of cycles N was fixed at 20000 at all infills. The triangular infill design exhibits a high fatigue life compared to the other infills.

Table 8: 60 filling percentage with different filling patterns

Material	UTS	infill density	Infill pattern	Stress	Life	Stress/uts
ABS	16.9	60%	Honeycomb	4	3.10E+03	0.2366864
				3.5	1.18E+04	0.2071006
				3	1.00E+06	0.1775148
ABS	16.9	60%	Rectilinear	3	6.19E+03	0.1775148
				2.5	4.77E+05	0.147929
				2	1.00E+06	0.1183432
ABS	16.9	60%	Triangle	3.5	4.73E+03	0.2071006
				3	4.98E+04	0.1775148
				2.2	1.00E+06	0.1301775

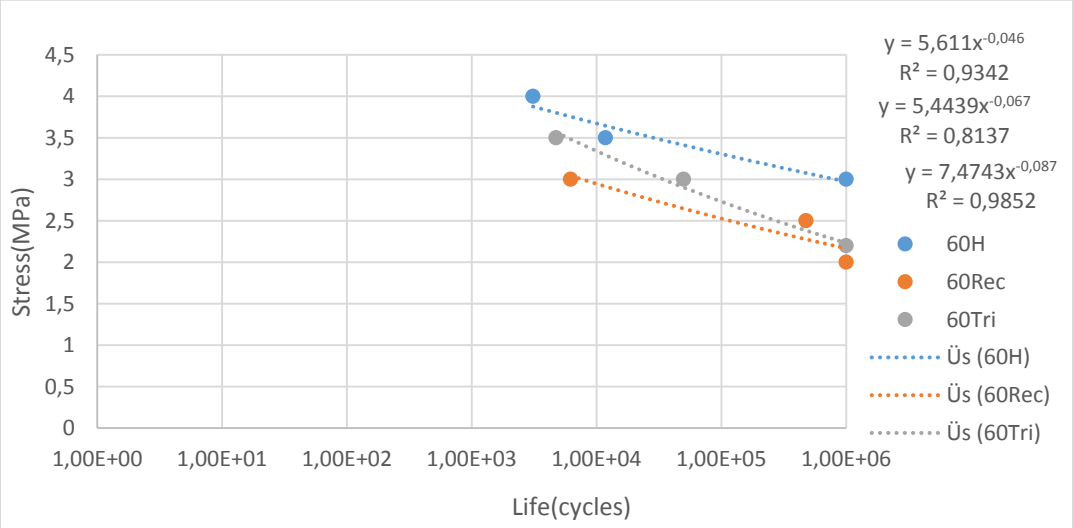

Figure 25: 60% infill density with ABS

Table 9: 60 infill density with honeycomb, rectilinear, and triangle filling patterns

Infill pattern	A	B	R^2
Honeycomb 60%	5.611	-0.046	0.9262
Rectilinear 60%	5.4439	-0.067	0.8425
Triangle 60%	7.4743	-0.087	0.9852

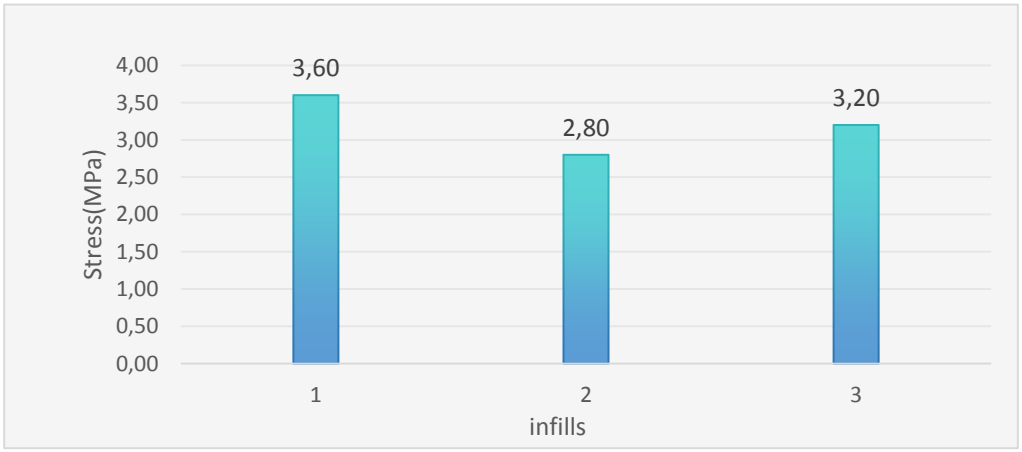

Figure 26: comparison among Honeycomb, Rectilinear, and Triangle to constant infill density of 60% ABS.

A comparison of the fatigue life based on the stress values for various infill patterns provided in Figure 25, 1 presents honeycomb (3.60 MPa), 2 presents rectilinear (2.8 MPa), and 3 presents triangle (3.20 MPa). The infills were printed at 60% infill density by ABS material. The life cycle was fixed at 20000 cycles to the all-infill patterns. The stress values show the maximum stress that a material can bear before breaking. Greater stress values indicate improved resilience to exhaustion. Among the patterns, the honeycomb infill has the greater stress value of 3.60 MPa, suggesting its superior fatigue life.

Table 10: 95 filling percentage with different filling patterns

Material	UTS	Infill density	Infill pattern	Stress	Life	Stress/uts
ABS	16.9	95%	Honeycomb	4	4.35E+03	0.2366864
				3.5	1.65E+04	0.2071006
				3	1.00E+06	0.1775148
			Rectilinear	4.5	3.26E+05	0.2662722
				4	7.35E+05	0.2366864
				3.5	1.00E+06	0.2071006
			Triangle	5	3.68E+05	2.96E-01
				4.5	7.60E+05	2.66E-01
				4	1.00E+06	2.37E-01

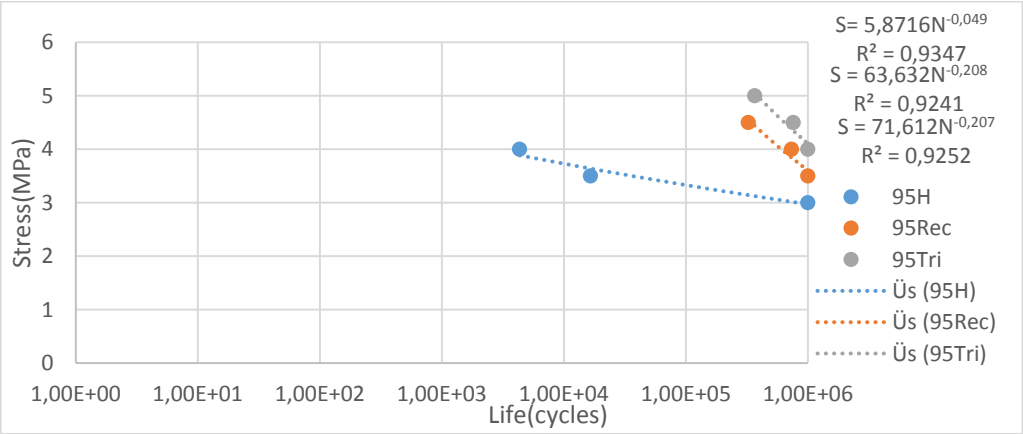

Figure 27: 95% infill density with ABS material

Table 11: Basquin's formula, 95 infill density with honeycomb, rectilinear, and Triangle infill pattern (ABS)

Infill pattern	A	B	R^2
Honeycomb 95%	5.8716	-0.049	0.9347
Rectilinear 95%	63.632	-0.208	0.9241
Triangle 95%	71.612	-0.207	0.9252

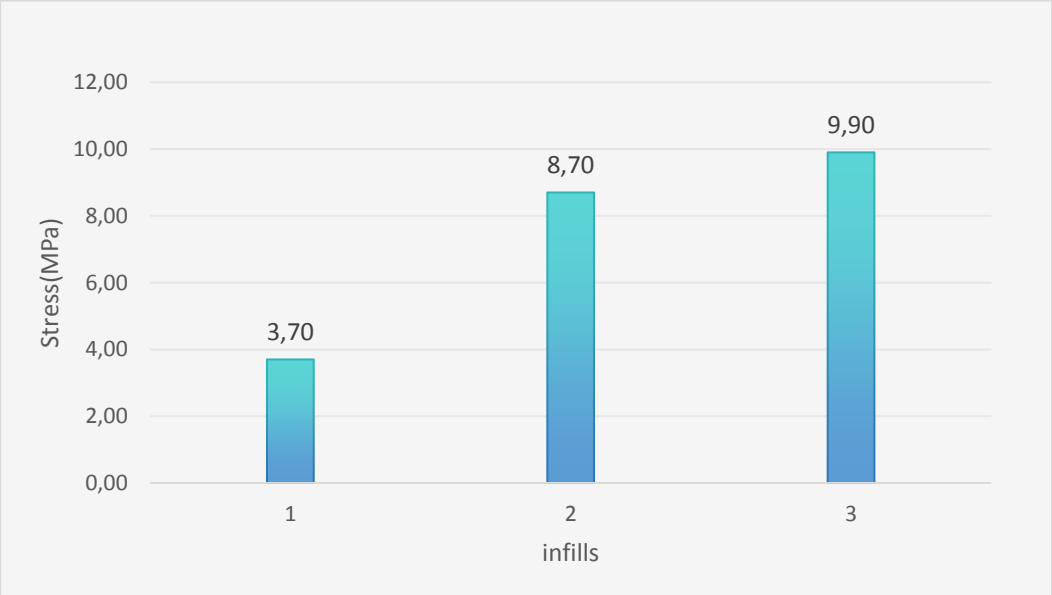

Figure 28: comparison among Honeycomb, Rectilinear, and Triangle to constant infill density of 95% ABS

Here is a comparison of the fatigue life based on the stress values for various infill patterns using the Figure 28, 1 presents honeycomb, 2 presents rectilinear, and 3 presents triangle. Both were printed at 95% infill density; the number of cycles were fixed at 20000 cycles by the ABS material. As a result, triangle infill pattern can carry a higher fatigue stress compared to rectilinear while honeycomb showed moderate resistance but is not as good as triangle infill.

4.2 Infill Density Comparison ABS

Table 12: honeycomb filling pattern with different filling percentages

Material	UTS	Infill density	Infill pattern	Stress (MPa)	Life (cycle)	Stress/uts
ABS	16.9	25%	Honeycomb	3.5	3013.3	0.2071006
				3	14413	0.1775148
				2.5	1.00E+06	0.147929
		60%	Honeycomb	4	3.10E+03	0.2366864
				3.5	1.18E+04	0.2071006
				3	1.00E+06	0.1775148
		95%	Honeycomb	4	4.35E+03	0.2366864
				3.5	1.65E+04	0.2071006
				3.1	1.00E+06	0.183432

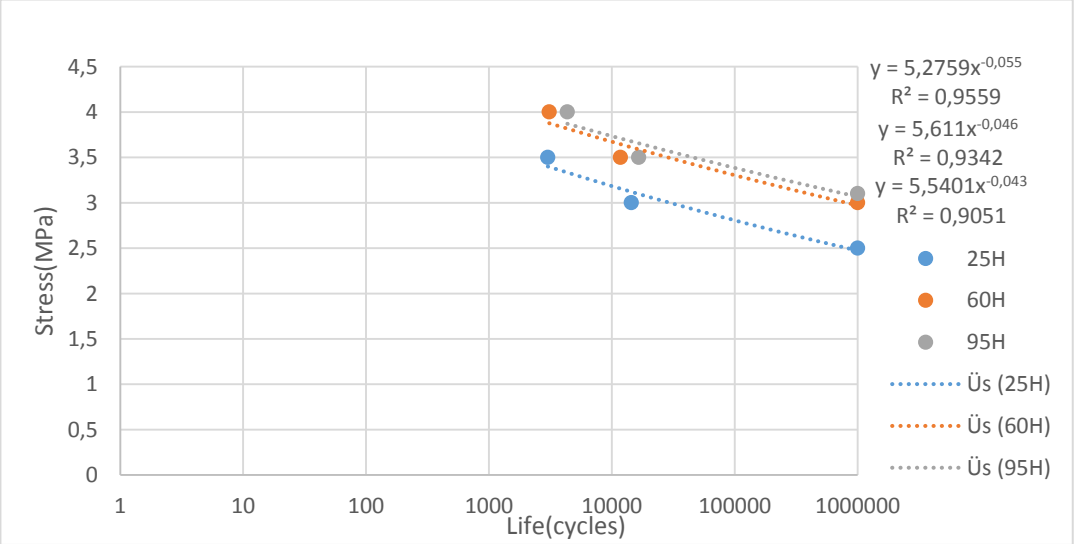

Figure 29: Honeycomb infill pattern with ABS material

Table 13: Basquin's formula parameters for Honeycomb infill pattern with 25, 60, and 95% infill densities (ABS)

Infill pattern	A	B	R^2
Honeycomb25%	5.2759	-0.055	0.9502
Honeycomb 60%	5.611	-0.046	0.9262
Honeycomb 95%	5.401	-0.048	0.9342

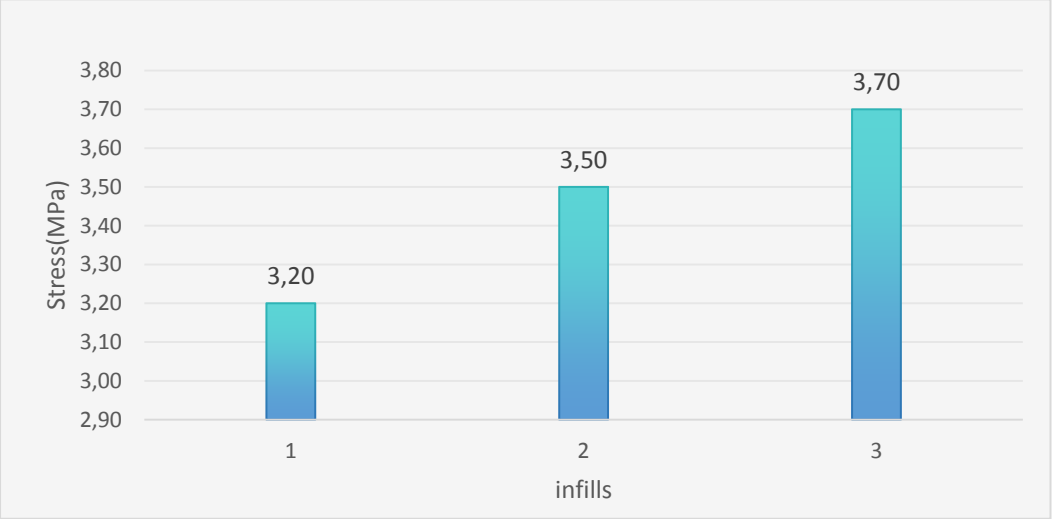

Figure 30: comparison among 25% honeycomb, 60% honeycomb, and 95% honeycomb. (ABS)

The fatigue life data for the three different infill densities 25H, 60H, and 95H are shown in Figure 30, 1 stands for 25% honeycomb, 2 stands for 60% honeycomb, while 3 stands for 95% honeycomb. Basquin's model parameters are displayed from Table 13, Figure 30 shows the predicted fatigue stress for various infill densities at a fatigue life of 20000 cycles.

Table 14: 25, 60 and 95 filling percentages with rectilinear filling pattern

Material	UTS	Infill density	Infill pattern	Stress	Life	Stress/uts
ABS	16.9	25%	Rectilinear	3.5	1.80E+03	0.2071006
				3	1.05E+04	0.1775148
				2.5	1.00E+06	0.147929
		60%	Rectilinear	3	6.19E+03	0.1775148
				2.5	4.77E+05	0.147929
				2	1.00E+06	0.1183432
		95%	Rectilinear	4.5	3.26E+05	0.2662722
				4	7.35E+05	0.2366864
				3.5	1.00E+06	0.2071006

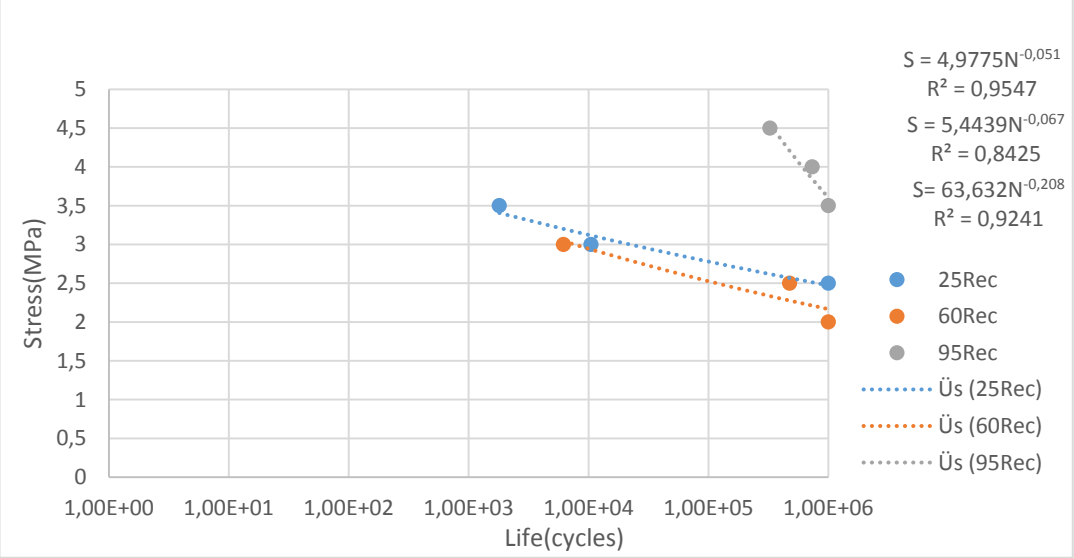

Figure 31: Rectilinear infill pattern with ABS

Table 15: Rectilinear infill patterns with 25, 60, and 95% infill densities (ABS).

Infill pattern	A	B	R^2
Rectilinear 25%	4.9775	-0.051	0.9547
Rectilinear 60%	5.4439	-0.067	0.8425
Rectilinear 95%	63.632	-0.208	0.9241

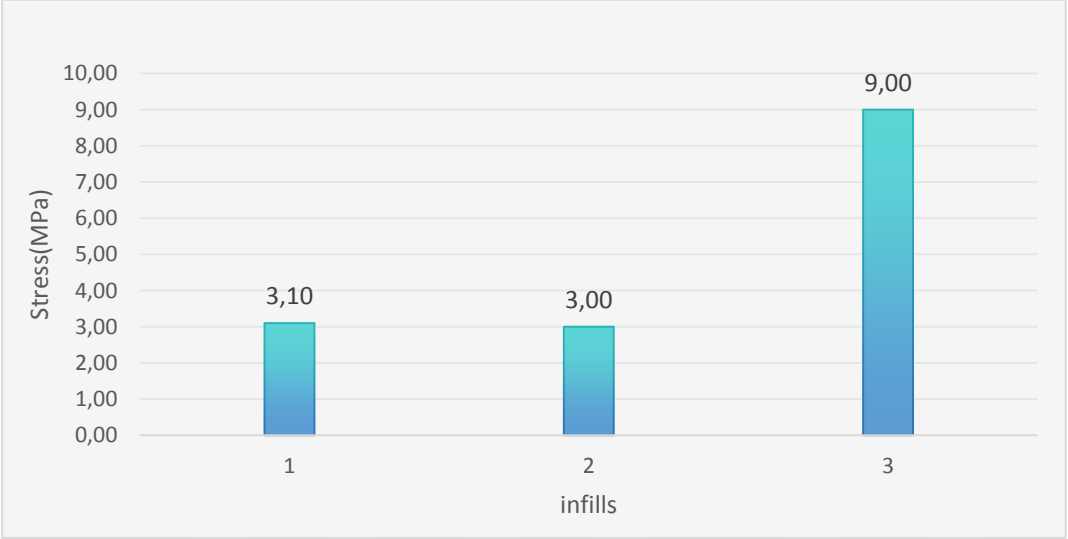

Figure 32: comparison among 25% honeycomb, 60% honeycomb, and 95% rectilinear. (ABS).

Figure 32 compared infill density to the constant infill patterns. 1 stands for 25% rectilinear, 2 stands for 60% rectilinear, while 3 stands 95% rectilinear. Basquin's model was used to calculate A, B and N from Table 15 where N was fixed at 20000 number of cycles. All three models were printed in ABS. 95% infill density has shown high resistance compare to 25% and 60%.

Table 16: 25, 60, and 95 filling percentage with triangle infill pattern

Material	UTS	Infill	Infill	Stress	Life	Stress/uts
ABS	16.9	25%	Triangle	3.5	4.27E+03	0.2071006
				3	3.60E+04	0.1775148
				2.5	1.00E+06	0.147929
		60%	Triangle	3.5	4.73E+03	0.2071006
				3	4.98E+04	0.1775148
				2	1.00E+06	0.1183432
		95%	Triangle	5	3.68E+05	2.96E-01
				4.5	7.60E+05	2.66E-01
				4	1.00E+06	2.37E-01

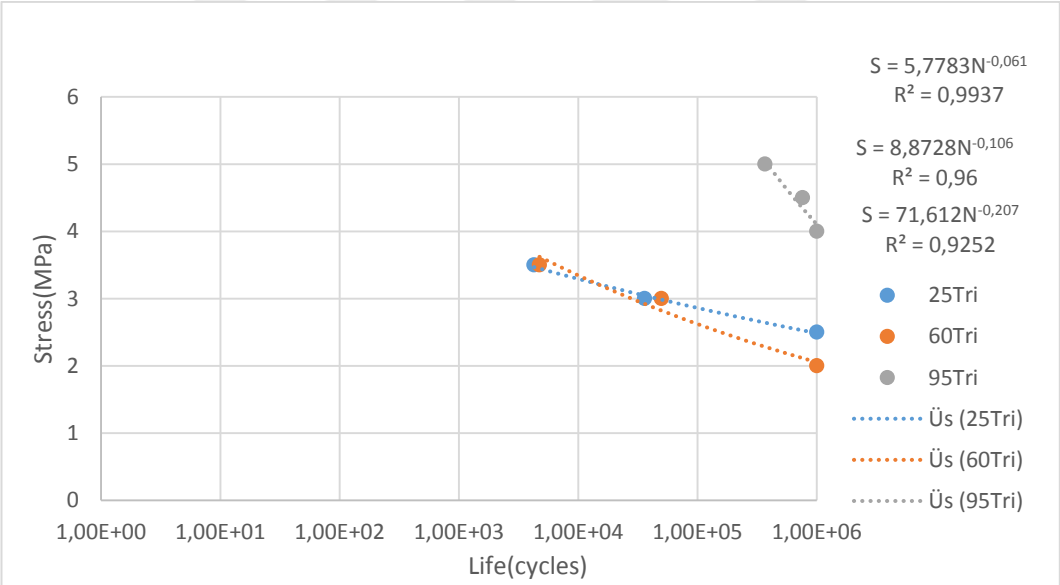

Figure 33: triangle infill with different infill percentages

Table 17: Triangle infill patterns with 25, 60, and 95% infill densities (ABS)

Infill density	A	B	R^2
25%	5.7783	-0,061	0,9937
60%	8.8728	-0,106	0.96
95%	71.612	-0,207	0,9252

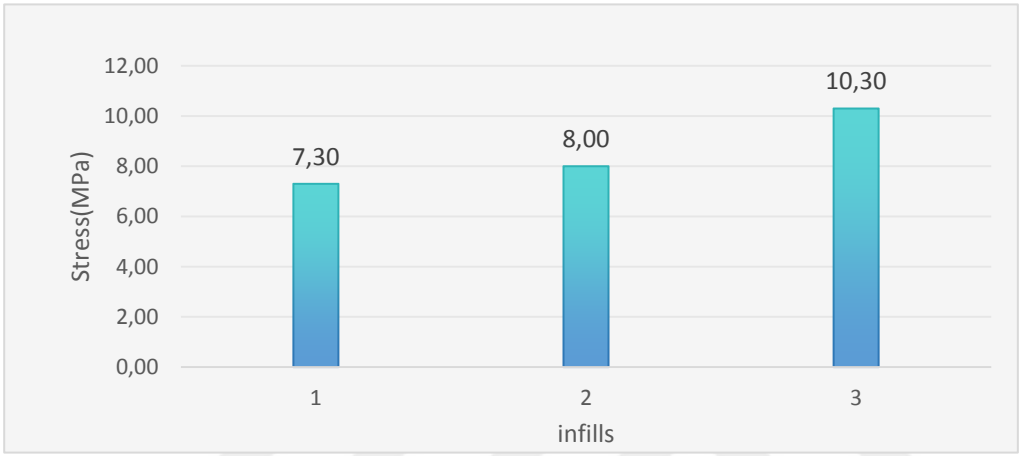

Figure 34: comparison among 25% honeycomb, 60% honeycomb, and 95% triangle. (ABS)

The fatigue life (life in cycles) of materials with varying infill densities 25%, 60%, and 95% was examined using the accompanying Figure 34 as a basis. As shown in Figure 34, 1 stands for 25% triangle, 2 stands for 60% triangle, while 3 stands for 95% triangle. Corresponding fatigue stress was calculated for a fatigue life of 20000 cycles for all cases. 95% infill pattern demonstrates high stress of 9.2 MPa while 25% were ranging between 3 and 4 MPa. While 60% was 8 and 9MPa.

4.3 Effect of the Infill Pattern and Density on Fatigue Properties of the FDM Printed PLA Material

Table 18: 25 infill percentage with honeycomb, rectilinear, and triangle filling pattern

Material	UTS	Infill density	Infill pattern	Stress	Life	Stress/uts
PLA	64	25%	Honeycomb	12	763.47	0.1875
				8.2	46105	0.128125
				4	1000000	0.0625
			Rectilinear	12	454.38	0.1875
				8	34832	0.125
				3.8	1000000	0.05937
			Triangle	12	6.87E+02	0.1875
				8	4.43E+04	0.125
				3.5	1.00E+06	0.0546875

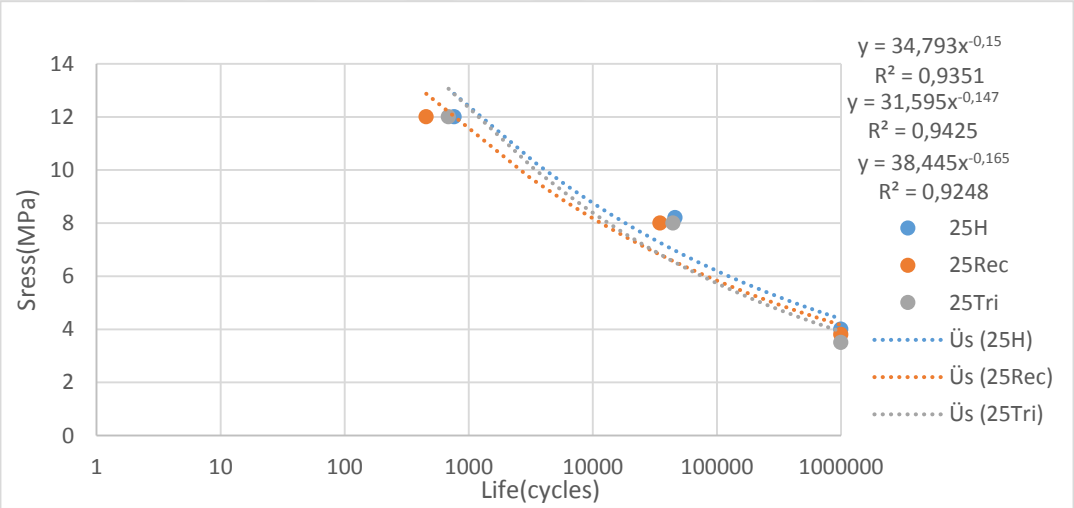

Figure 35: 25% Infill density with honeycomb, rectilinear, and triangle infill pattern PLA

Table 19: Basquin's formula parameters for 25% infill density with honeycomb, rectilinear, and triangle infill patterns (PLA)

Infill pattern	A	B	R^2
Honeycomb 25%	34.625	-0.15	0.9508
Rectilinear 25%	30.139	-0.14	0.9538
Triangle 25%	33.594	-0.148	0.9506

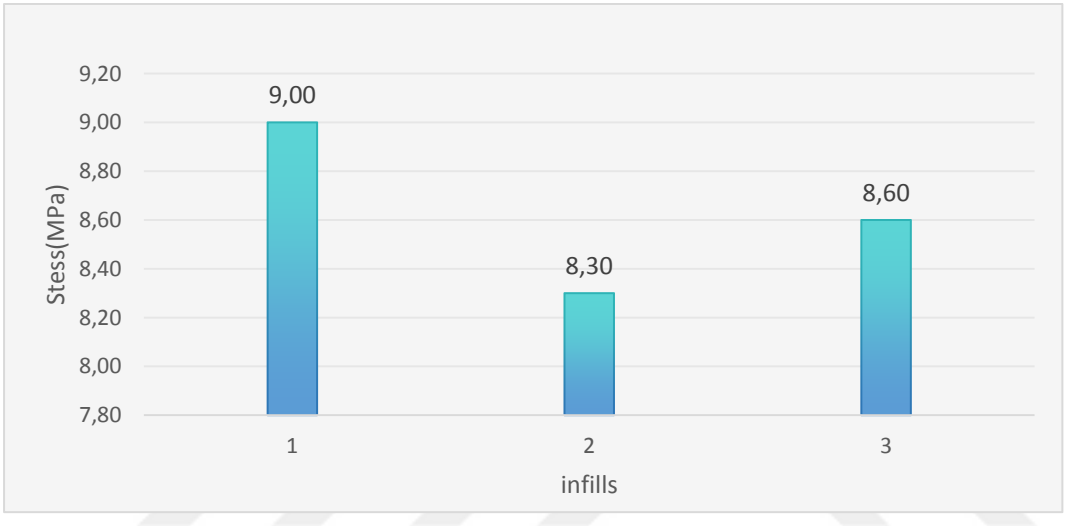

Figure 36: comparison among Honeycomb, Rectilinear, and Triangle to constant infill density of 25% PLA

Here is a comparison of the fatigue life based on stress values for various infill patterns produced with 25% infill density using PLA material, based on the provided figure. 1 presents honeycomb at stress level of (9.0MPa), 2 presents rectilinear at a stress level of (8.30MPa), and triangle at a stress of (8.60MPa). Life cycles were fixed at 20000 cycles.

Among these three patterns, the honeycomb infill (1) has the highest fatigue life, with a stress value of 9.00 MPa.

Table 20: 25 infill percentage with honeycomb, rectilinear, and triangle filling pattern

Material	UTs	Infill density	Infill pattern	Stress	Life	Stress/uts
PLA	64	60%	Honeycomb	14	4.89E+02	0.21875
				10	2.59E+04	0.15625
				5	9.13E+05	0.078125
				3	1.00E+06	0.046875
			Rectilinear	10	1.86E+03	0.15625
				5	1.86E+05	0.078125
				3	1.00E+06	0.046875
			Triangle	10	7.14E+03	0.15625
				5	4.47E+05	0.078125
				4	1.00E+06	0.0625

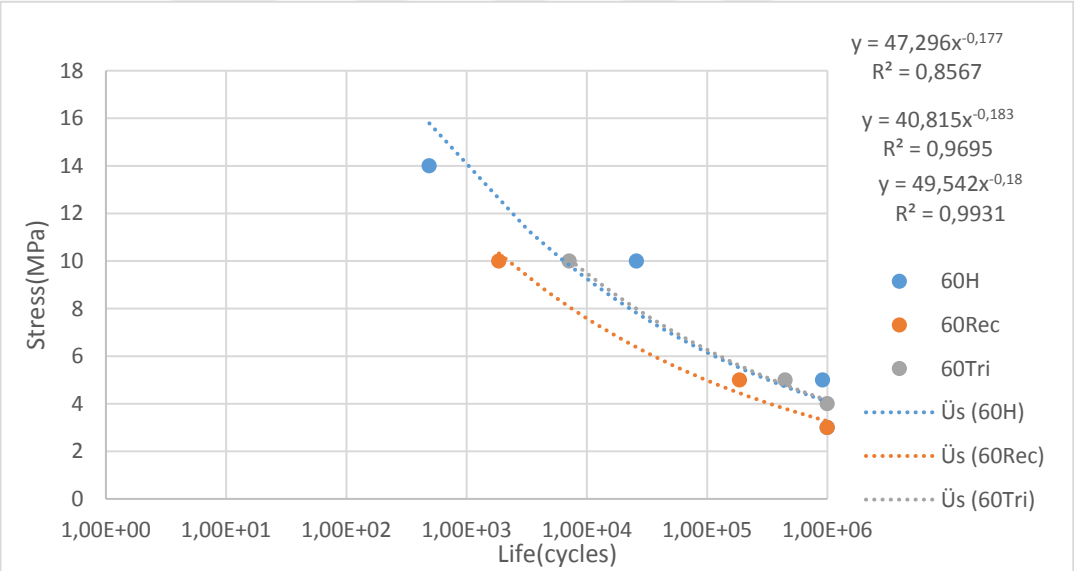

Figure 37: 60% Infill density with honeycomb, rectilinear, and triangle infill pattern PLA

Table 21: 60% infill density with honeycomb, rectilinear, and triangle infill patterns (PLA) material

Infill pattern	A	B	R^2
Honeycomb 60%	47.296	-0.177	0.893
Rectilinear 60%	40.815	-0.183	0.9845
Triangle 60%	49.542	-0.18	0.9931

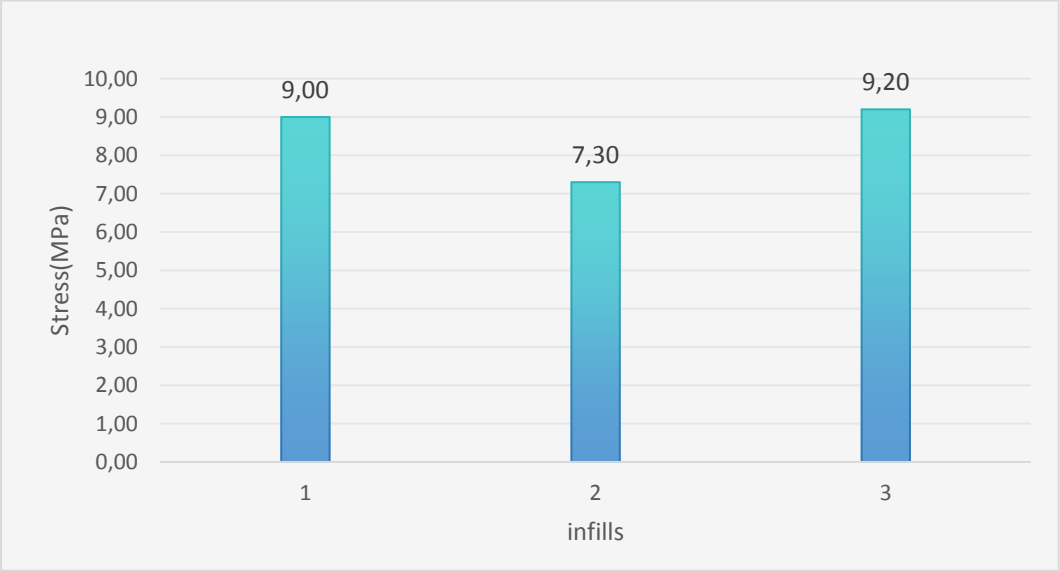

Figure 38: comparison among Honeycomb, Rectilinear, and Triangle to constant infill density of 60% PLA

Figure 38 presents a comparison among infill patterns. 1 present honeycomb, 2 present rectilinear and 3 present triangles. All patterns were compared at the same infill density of 60% with same number of cycles. They were all printed on the same material of PLA. As we can see, number 3 which represents triangle infill pattern, has a high fatigue stress of 9.2 MPa compared to the honeycomb and rectilinear.

Table 22: 95 filling percentage with different filling patterns

Material	UTS	Infill density	Infill pattern	Stress	Life	Stress/uts
PLA	64	95%	Honeycomb	15	1.10E+02	0.234375
				10	3.01E+04	0.15625
				5	1.00E+06	0.078125
			Rectilinear	10	1.06E+03	0.15625
				5	1.54E+05	0.078125
				3	1.00E+06	0.046875
			Triangle	10	5.77E+03	0.15625
				5	3.68E+05	0.078125
				3.5	1.00E+06	0.054687

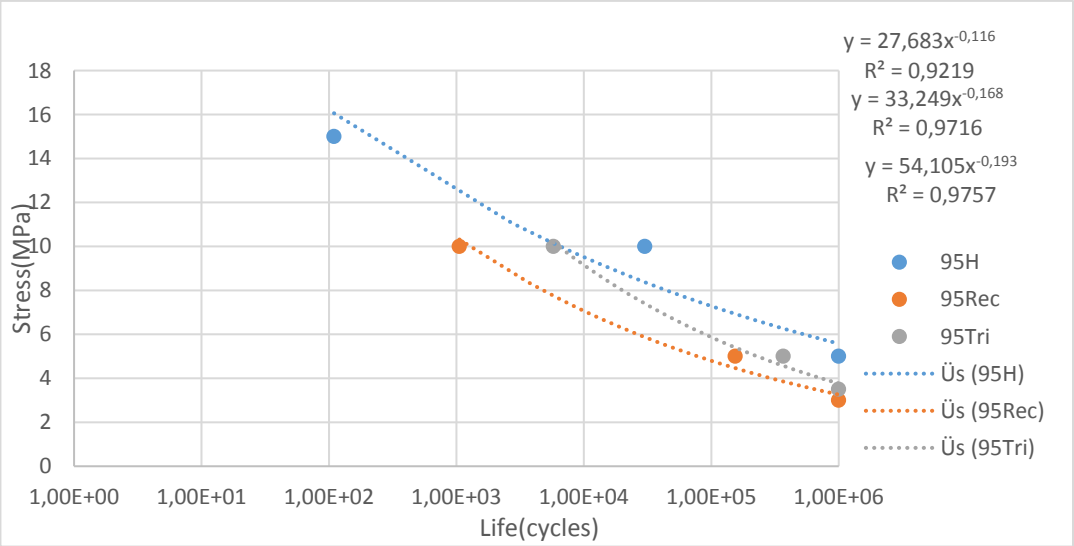

Figure 39: 95% Infill density with honeycomb, rectilinear, and triangle infill pattern PLA

Table 23: Basquin's formula parameters for 95% infill density with honeycomb, rectilinear, and triangle infill patterns (PLA)

Infill pattern	A	B	R^2
Honeycomb 95%	27.683	-0.116	0.9323
Rectilinear 95%	33.249	-0.168	0.9854
Triangle 95%	54.105	-0.193	0.9757

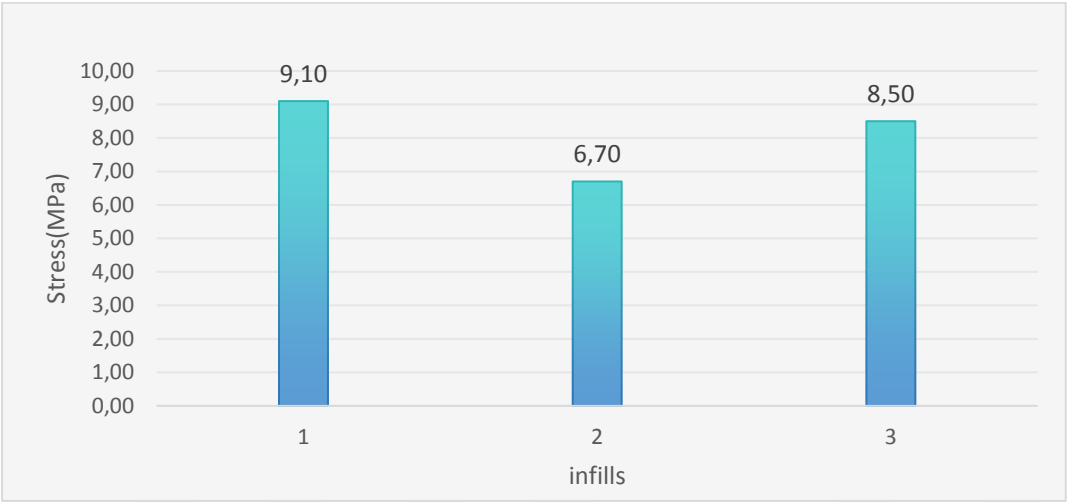

Figure 40: comparison among Honeycomb, Rectilinear, and Triangle to constant infill density of 95% PLA

Based on Figure 40, Based on Figure 44, to examine the filling patterns in the context of 3D printing that resisted much better while retaining a constant infill density of 95% PLA with the same 20000 cycles, as you can see, 1 represents a honeycomb, 2 represents a rectilinear, and 3 represents a triangle. Number 1, honeycomb is higher with a stress of 9.1 MPa, which means that it has a better fatigue life compared to the rectilinear and triangle infills.

4.4 Effect of the Infill Pattern and Density on Fatigue Properties of the FDM Printed PA12CF Material

Table 24: 25% filling percentage and filling patterns

Material	UTS	Infill density	Infill pattern	Stress	Life	Stress/uts
PA12CF	40.2	25%	Honeycomb	8	1584.2	0.199004975
				7	16284	0.174129353
				6	45719	0.149253731
			Rectilinear	7	4981.3	0.174129353
				6.5	17557	0.161691542
				5	45719	0.124378109
			Triangle	8	1343.3	0.199004975
				7	14031	0.174129353
				5.5	45719	0.13681592

Table 24 displays the data on mechanical properties of material PA12CF. Ultimate tensile strength is 40.2 MPa. Infill patterns compared were honeycomb, rectilinear, and triangle at constant infill density 25%. life column displays fatigue life after stress has applied by simulation. Stress/uts. This ratio shows the material's proximity to its ultimate strength when stress is applied.

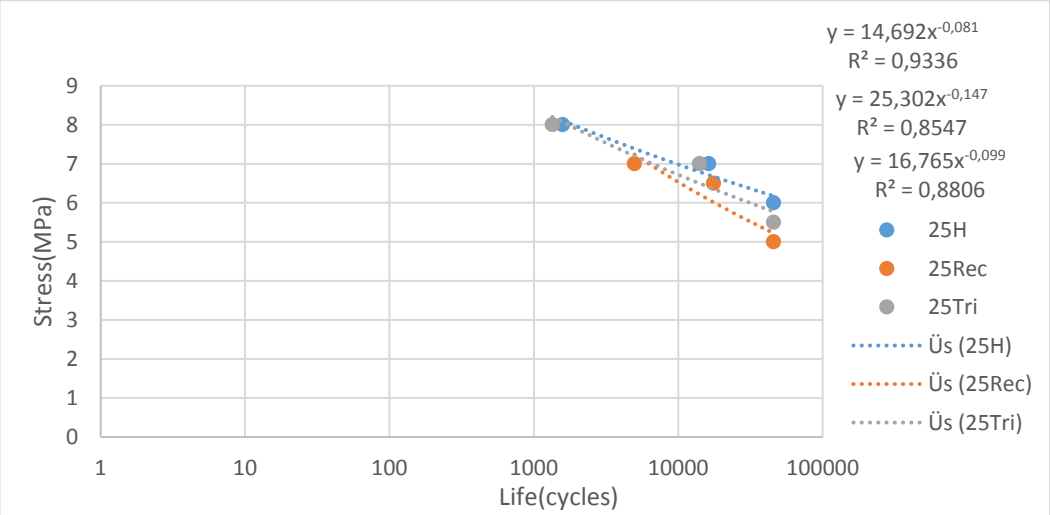

Figure 41: Comparison of filling patterns and 25% filled percentage

With a 25% infill density, this plot illustrates the relationship between stress (measured in MPa) and the number of life cycles for three distinct infill patterns: triangle (Tri), rectilinear (Rec), and honeycomb (H). All three patterns exhibit a power-law relationship, which is to be expected: stress decreases as life cycles grow. This suggests that materials under less stress can withstand a greater number of cycles before failing.

Table 25: 25 infill percentage with filling patterns

infill	A	B	R^2
Honeycomb 25	14.692	-0.081	0.9387
Rectilinear 25	25.302	-0.147	0.8448
Triangle 25	16.765	-0.099	0.8806

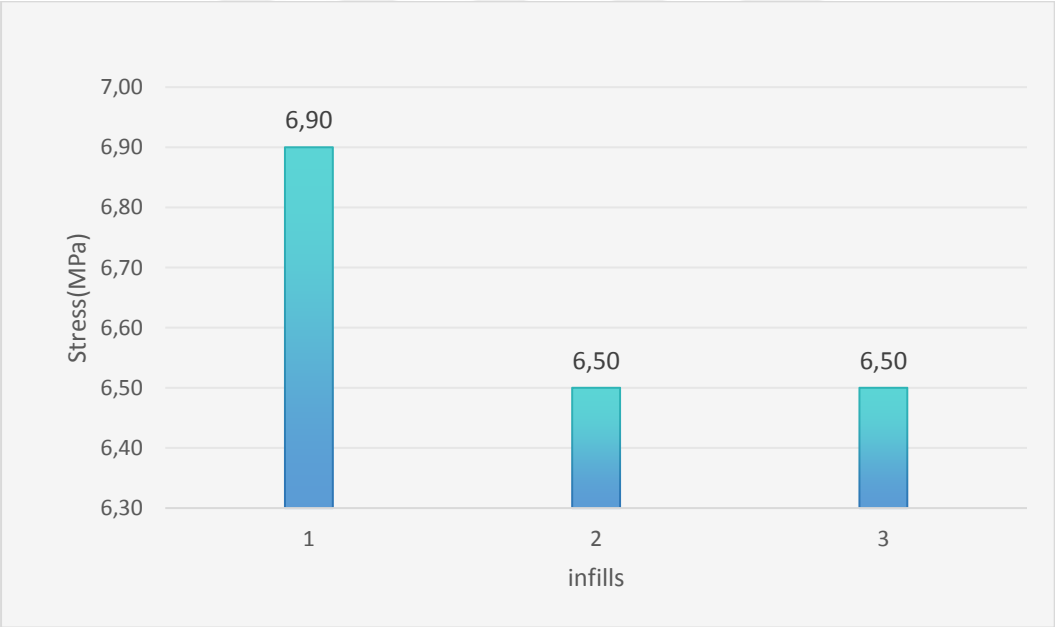

Figure 42: comparison among Honeycomb, Rectilinear, and Triangle to constant infill density of 25% PA12CF

The fatigue lives of specimens with a 25% infill density employing various infill patterns under cyclic loading are shown in Figure 42. The comparison was made due to verify the best infill pattern among honeycomb, rectilinear, and triangle. 1 presents honeycomb at a stress of (6.9MPa), 2 presents rectilinear at a stress of (6.5MPa), and 3 presents triangle at a stress of (6.5MPa). The comparison was made at the constant

number of cycles of cycles. The honeycomb infill pattern has high stress compare to the two-rest, meaning that it has a high fatigue life compare to the rectilinear and triangle.

Table 26: 60% filling percentage with filling patterns

Material	UTS	Infill density	Infill pattern	Stress	Life	Stress/uts
PA12CF	40.2	60%	Honeycomb	9	1915.1	0.223880597
				8	14888	0.199004975
				6	45719	0.149253731
			Rectilinear	7	1819.7	0.174129353
				6	25894	0.149253731
				5	45719	0.124378109
			Rectilinear	8	1215.8	0.199004975
				7	12825	0.174129353
				5.5	45719	0.13681592

Table 26 displays the data on mechanical properties of material PA12CF. Ultimate tensile strength is 40.2 MPa. Honeycomb infill patterns, rectilinear, and triangle were compared to constant infill density 60%. Life column displays fatigue life after stress has applied by simulation. Stress/uts. This ratio shows the material's proximity to its ultimate strength when stress is applied.

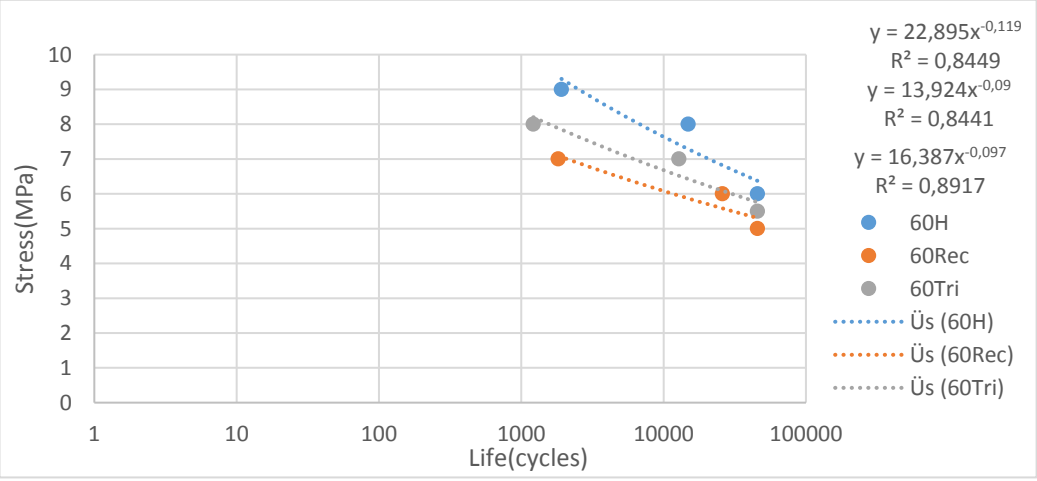

Figure 43: Comparison of filling patterns and 60% filled percentage

With a 60% infill density, three infill patterns Honeycomb (H), Rectilinear (Rec), and Triangle (Tri) are depicted in this image along with their corresponding relationships to stress (in MPa) and life cycles. As the number of life cycles rises, all three infill schemes show a decrease in stress. Blue presents honeycomb, orange presents rectilinear, and gray presents triangle infill patterns.

Table 27: 60% infill percentage with different filling patterns

Infill	A	B	R^2
Honeycomb 60	22.895	-0.119	0.845
Rectilinear 60	13.924	-0.09	0.8637
Triangle 60	16.387	-0.097	0.8917

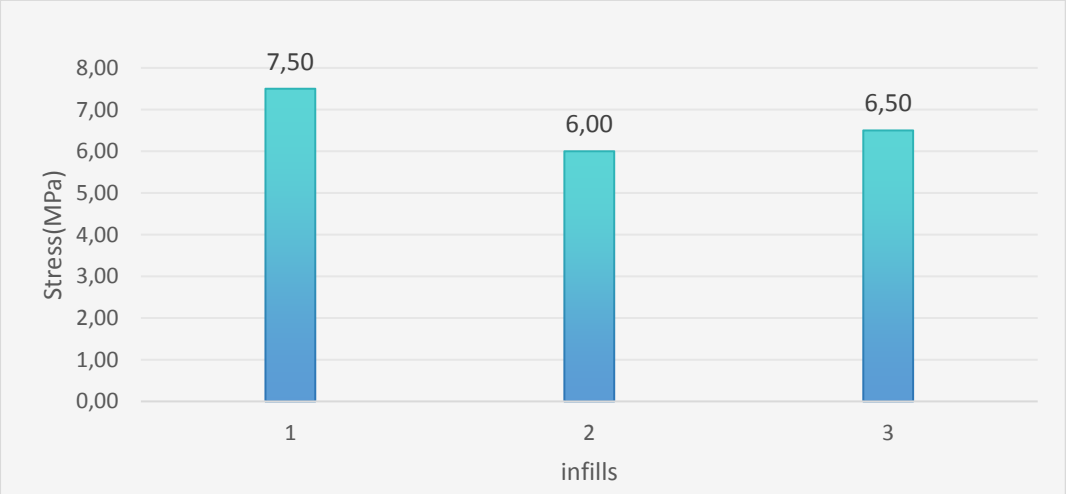

Figure 44: comparison among Honeycomb, Rectilinear, and Triangle to constant infill density of 60% PA12CF

The fatigue life of specimens with a 60% infill density employing rectilinear, triangular, and honeycomb infill patterns under cyclic stress was compared in Figure 44, 1 stands for honeycomb, 2 stands for rectilinear, while 3 stands for triangle infill. The comparison was made using a Basquin's model A and B displayed in Table 27, while N was 20000 cycles applied to all infill patterns. The models were simulated using PA12CF as a material. Honeycomb infill patterns showed high fatigue life with a stress of 7.5 MPa.

Table 28: 95% filling percentage with filling patterns

Material	UTS	Infill density	Infill pattern	Stress	Life	Stress/uts
PA12CF	40.2	95%	Honeycomb	9	1711.7	0.223880597
				8	13435	0.199004975
				6	45719	0.149253731
			Rectilinear	7	1067.7	0.174129353
				6	16111	0.149253731
				5	45719	0.124378109
			Triangle	8	922.5	0.199004975
				7	10003	0.174129353
				5.5	45719	0.13681592

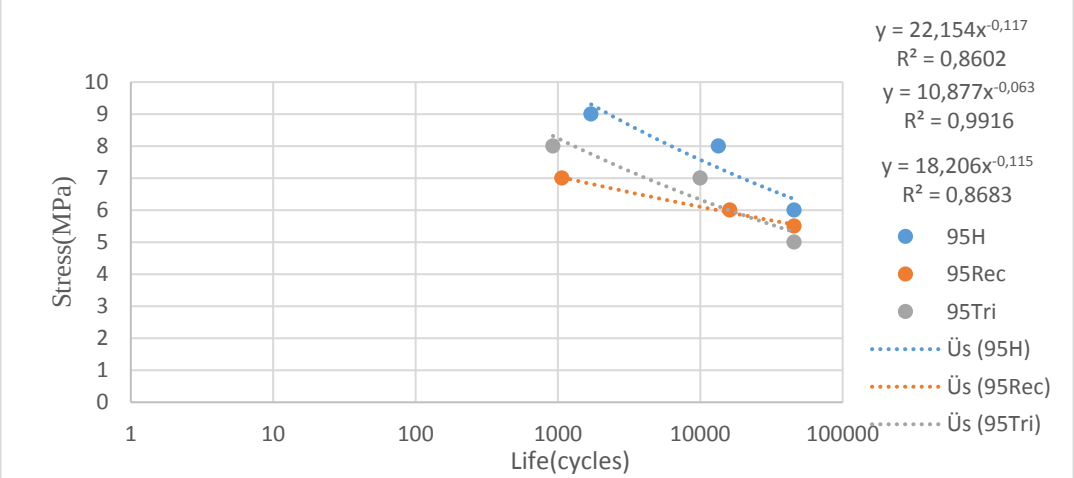

Figure 45: Comparison of filling patterns with the 95% filled percentage

Table 29: 95% infill percentage with different filling patterns

Infill	A	B	R^2
Honeycomb 95	22.154	-0.117	0.8588
Rectilinear 95	10.877	-0.063	0.9916
Triangle 95	13.233	-0.072	0.9732

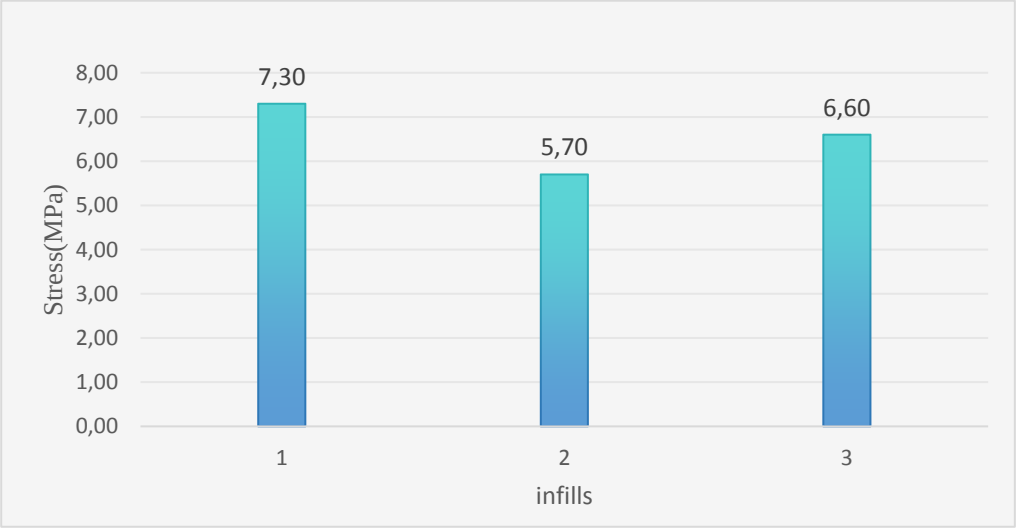

Figure 46: comparison among Honeycomb, Rectilinear, and Triangle to constant infill density of 95% PA12CF

Compared to Rectilinear and Triangle patterns, Honeycomb exhibits the best fatigue life, enduring more cycles before it failed as indicated by 1. Rectilinear showed lower fatigue life and it indicated by 2. The triangle showed a moderate as indicated by 3 in Figure 46.

4.5 Comparison Among Materials, ABS, PLA, and PA12CF

Table 30: comparison among materials used (Honeycomb)

Material	Infill pattern	Infill density	N-cycles	A	B
ABS				5.8716	-0.049
PLA	Honeycomb	95%	20000	27.683	-0.116
PA12CF				22.154	-0.117
ABS				63.632	-0.208
PLA	Rectilinear	95%	20000	33.249	-0.168
PA12CF				12.679	-0.083
ABS				71.612	-0.207
PLA	Triangle	95%	20000	65.925	-0.214
PA12CF				13.233	-0.072

Table 30 combines materials, ABS, PLA, and PA12CF to 95% infill density. Number of cycles was fixed to 20000 cycles. Comparison of material done to infill patterns, honeycomb, rectilinear, and triangle.

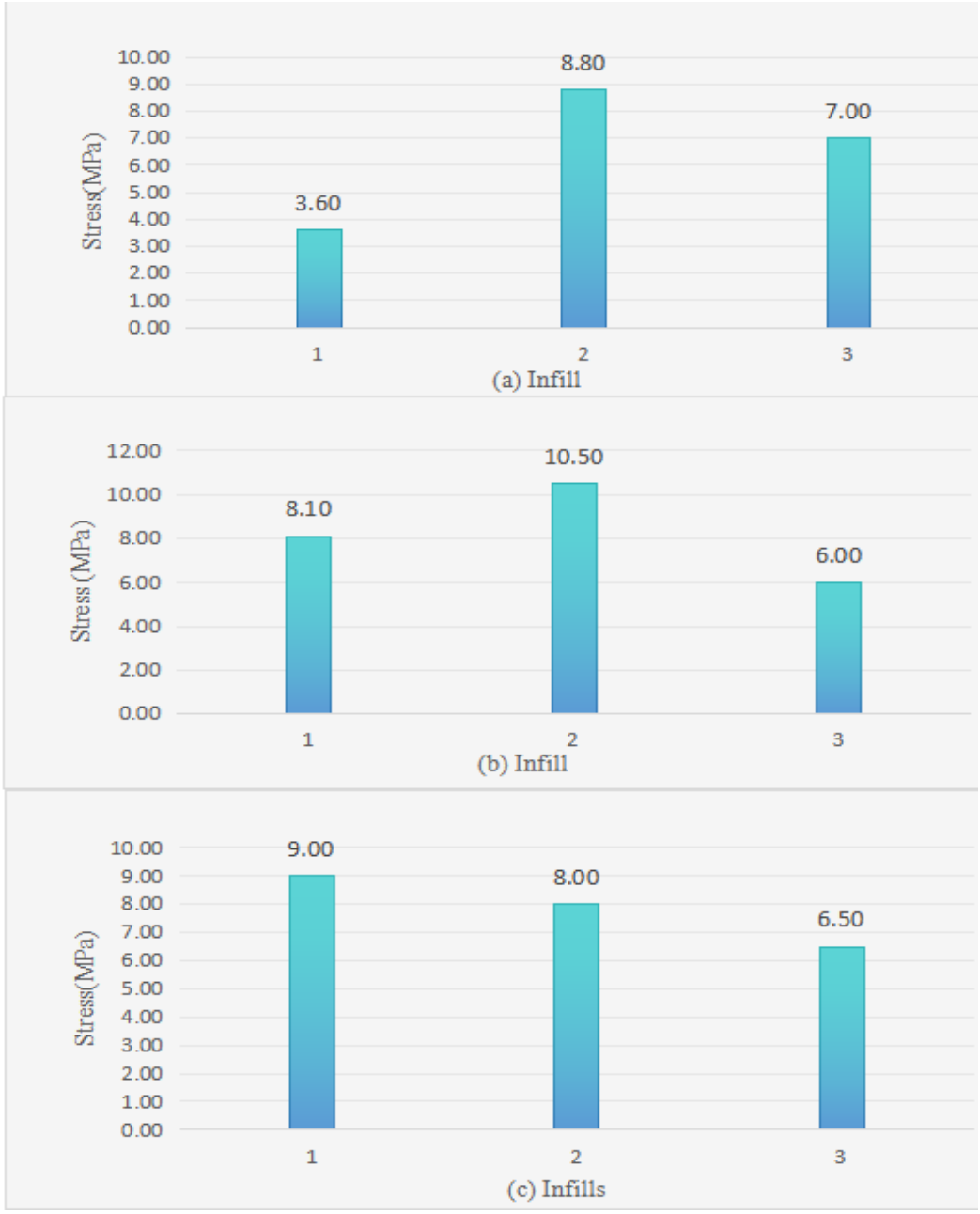

Figure 47: Comparison of ABS PLA and PA12 CF

Figure 47 shows comparison among material, ABS, PLA, and PA12CF. (A) presents comparison of materials to 95 honeycombs, 1 stands for 95 honeycomb ABS, 2

stands for 95 honeycomb PLA, 3 stands for 95 honeycomb PA12CF. (B) presents comparison of materials to 95 rectilinear, 1 stands for 95 rectilinear ABS, 2 stands 95 rectilinear PLA while 3 stands for 95 rectilinear PA12CF. (C) presents comparison of materials to 95 triangle, 1 stands for 95 triangle ABS, 2 stands 95 triangle PLA and 3 stands 95 triangle PA12CF.

(A) Show that PLA has high stress of 8.8MPa which means high fatigue life compare to ABS and PA12CF.

(B) Show also that PLA has high stress applied of 10.5MPa. It indicates high fatigue compared to others.

(C) Show ABS as fatigue resistance material among PLA and PA12CF as it indicates high stress of 9MPa.

CHAPTER 5

CONCLUSION

The purpose of this study was to investigate the potential effects of various material types, infill densities, and patterns on the fatigue life of 3D-printed parts.

The study's findings made it abundantly evident that a key factor in determining the fatigue life of 3D-printed composites is the infill pattern selection. The honeycomb infill design showed the longest fatigue life out of PA12CF and PLA while on ABS triangle and honeycomb both showed the same fatigue life. The enhanced performance of this pattern can be ascribed to its geometric arrangement, which offers improved structural support and load distribution. The increased fatigue resistance of the honeycomb infill is due to its capacity to distribute stress more uniformly throughout the structure. However, in some cases, like 95% and 25% infill density via ABS the triangle showed a high fatigue life compared to other infills. On the other hand, although they are still widely utilized, the rectilinear layouts did not fare as well under fatigue loading circumstances.

In addition, the effect of various infill densities on the fatigue life of 3D printed parts was also investigated. It was discovered that the material's resilience to fatigue is much enhanced by a higher infill density. Under the fatigue loading, an infill density of 95% performed better than densities of 25% and 60%. With a high infill density of 95%, the interior structures are close to each other which is helpful in supporting stress. The composite's overall mechanical qualities are improved by this thick structure, which also lengthens its lifespan. On the other hand, it was discovered that, despite using less material and taking less time to print, lower infill densities, such 25% and 60%, compromised the composite's fatigue life. Because of these lower densities, the interior structure is more porous and more prone to stress concentrations and crack propagation from repetitive loading. The results showed that as you increase filling density, the fatigue life will also be high and vice-visa.

The comparison was made on all infill pattern (25H, 60H, and 95H), (25REC, 60REC, and 95REC), and (25TRI, 60TRI, and 95TRI). In all these tests 95% infill density demonstrates better performance.

Furthermore, the study looked at several materials' performance, particularly PLA, ABS, and PA12CF in addition to infill patterns and densities. In comparison to ABS, PLA material exhibited superior fatigue performance. This is explained by PLA on honeycomb infill pattern showed high fatigue, intrinsic material qualities, which include increased rigidity and improved layer bonding between printed layers. ABS dominated both PLA and PA12CF on both rectilinear and triangle infill. Since of its superior layer adhesion, ABS has a longer fatigue life since there is less chance of inter-layer decontamination under cyclic stress. PA12CF, this study found that carbon fiber is good to use in additive manufacturing while it less resistance according to this study.

The field of composite materials and 3D printing will be significantly impacted by the study's conclusions in a number of ways. Given that high infill density and the triangle infill pattern have been shown to be more effective at extending fatigue life, these optimization techniques ought to be taken into account in applications where fatigue resistance and long-term durability are crucial. Adopting these optimal printing conditions can greatly extend the product's service life, especially for sectors and applications like aerospace, automotive, and medical devices that depend on 3D-printed components subjected to cyclic loads.

Moreover, the choice of material is also very important. Even though ABS and PLA performed better in this study, the material selection process should still be based on the particular needs of the application, taking into account aspects like cost, environmental resistance, and mechanical qualities. To further extend the fatigue life of 3D-printed structures, future studies may investigate different materials and composite reinforced blends.

To sum up, this thorough analysis of how infill patterns affect 3D printed composite fatigue life has highlighted how crucial it is to choose the right infill patterns,

densities, and materials. When combined with a high infill density, the honeycomb infill pattern greatly improves the fatigue resistance of 3D-printed composites. Furthermore, ABS and PLA materials performs better in terms of fatigue life than PA12CF, which makes it a better option for applications requiring a high level of durability. These discoveries further the development of additive manufacturing technology by opening the door to stronger and more dependable 3D-printed structures.

REFERENCES

1. Gibson, I., et al., *Additive manufacturing technologies*. Vol. 17. 2021: Springer.

2. Wong, K.V. and A. Hernandez, *A review of additive manufacturing.* International scholarly research notices, 2012. **2012**.

3. Huang, S.H., et al., *Additive manufacturing and its societal impact: a literature review.* The International journal of advanced manufacturing technology, 2013. **67**: p. 1191-1203.

4. Monfared, V., et al., *Science and Technology of Additive Manufacturing Progress: Processes, Materials, and Applications.* Metals and Materials International, 2023. **29**(12): p. 3442-3470.

5. Arcese, G., et al. *THE IMPACT OF ICT-BASED TECHNOLOGIES ON THE DIFFUSION OF A TECHNO-ECONOMICAL MODEL: THE CASE OF SHARING ECONOMY*. in *Presidente del Congresso*. Università degli Studi della Tuscia.

6. Wohlers, T., et al., *Wohlers Report 2020 3D Printing and Additive Manufacturing State of the Industry*. 2020.

7. Campbell, T., et al., *Could 3D printing change the world.* Technologies, Potential, and Implications of Additive Manufacturing, Atlantic Council, Washington, DC, 2011. **3**(1): p. 18.

8. Chua, C.K. and K.F. Leong, *3D Printing and additive manufacturing: Principles and applications (with companion media pack)-of rapid prototyping*. 2014: World Scientific Publishing Company.

9. Kumar, S., B.L. Wardle, and M.F. Arif, *Strength and performance enhancement of bonded joints by spatial tailoring of adhesive compliance via 3D printing.* ACS applied materials & interfaces, 2017. **9**(1): p. 884-891.

10. Islam, M.K., *The Dynamic Response of Additively Manufactured Bioinspired Structures*. 2023, UNSW Sydney.

11. Kargar, E. and A. Ghasemi-Ghalebahman, *Experimental investigation on fatigue life and tensile strength of carbon fiber-reinforced PLA composites based on fused deposition modeling.* Scientific Reports, 2023. **13**(1): p. 18194.

12. Schneck, M., et al., *Evaluating the use of additive manufacturing in industry applications.* Procedia CIRP, 2019. **81**: p. 19-23.

13. Kumar, S., & Nair, G, *Additive manufacturing for automotive applications. In Additive Manufacturing Handbook (pp. 297-318). CRC Press.* 2018.

14. Rosen, D.W., *Computer-aided design for additive manufacturing of cellular structures.* Computer-Aided Design and Applications, 2007. **4**(5): p. 585-594.

15. Herderick, E. *Additive manufacturing of metals: A review*. in *Mater. Sci. Technol. Conf. Exhib*. 2011.

16. Ngo, T.D., et al., *Additive manufacturing (3D printing): A review of materials, methods, applications and challenges.* Composites Part B: Engineering, 2018. **143**: p. 172-196.

17. Gibson, I., et al., *Direct digital manufacturing.* Additive manufacturing technologies: 3D printing, rapid prototyping, and direct digital manufacturing, 2015: p. 375-397.

18. Wei, Y., et al., *Stereolithography-based additive manufacturing of high-performance osteoinductive calcium phosphate ceramics by a digital light-processing system.* ACS Biomaterials Science & Engineering, 2020. **6**(3): p. 1787-1797.

19. Phillips, B.T., et al., *Additive manufacturing aboard a moving vessel at sea using passively stabilized stereolithography (SLA) 3D printing.* Additive Manufacturing, 2020. **31**: p. 100969.

20. Xu, X., et al., *Stereolithography (SLA) 3D printing of a bladder device for intravesical drug delivery.* Materials Science and Engineering: C, 2021. **120**: p. 111773.

21. Charoo, N.A., et al., *Selective laser sintering 3D printing–an overview of the technology and pharmaceutical applications.* Drug development and industrial pharmacy, 2020. **46**(6): p. 869-877.

22. Padmakumar, M., *Additive manufacturing of tungsten carbide hardmetal parts by selective laser melting (SLM), selective laser sintering (SLS) and binder jet 3D printing (BJ3DP) techniques.* Lasers Manuf. Mater. Process, 2020. **7**(3): p. 338-371.

23. Charoo, N.A., et al, *Selective laser sintering 3D printing–an overview of the technology and pharmaceutical applications. Drug development and industrial pharmacy.* 2020.

24. Allahham, N.A., Taheri, S. A., Alzoubi, K. H., & Qiblawey, H, *Additive Manufacturing Technologies: State of the Art and Applications in Drug Delivery. AAPS PharmSciTech.* 2020.

25. Gibson, I., Rosen, D. W., & Stucker, B. , *Additive Manufacturing Technologies: 3D Printing, Rapid Prototyping, and Direct Digital Manufacturing. Springer. This comprehensive text covers the principles and applications of different additive manufacturing technologies, with a significant focus on FDM.* 2014.

26. Wang, J., Goyanes, A., Gaisford, S., & Basit, A. W, *Application of 3D printing technology on drug delivery: Review and advances. Drug Delivery and Translational Research.* 2021.

27. Sood, A.K., Ohdar, R. K., & Mahapatra, S. S, *Parametric appraisal of mechanical property of fused deposition modelling processed parts. Materials & Design.* 2010.

28. Quero, R.F., et al., *Understanding and improving FDM 3D printing to fabricate high-resolution and optically transparent microfluidic devices.* Lab on a Chip, 2021. **21**(19): p. 3715-3729.

29. Mohamed, O.A., Masood, S. H., & Bhowmik, J. L, *Optimization of fused deposition modeling process parameters for dimensional accuracy using I-optimality criterion. Measurement.* 2015.

30. Alsoufi, M.S. and A.E. Elsayed, *How surface roughness performance of printed parts manufactured by desktop FDM 3D printer with PLA+ is influenced by measuring direction.* Am. J. Mech. Eng, 2017. **5**(5): p. 211-222.

31. Quodbach, J., et al., *Quality of FDM 3D printed medicines for pediatrics: considerations for formulation development, filament extrusion, printing process and printer design.* Therapeutic Innovation & Regulatory Science, 2021: p. 1-19.

32. Smith, J.A., & Doe, R. B., *Enhancing polymer composites with fiber reinforcements: Mechanical and thermal benefits. Journal of Composite Materials.* 2020.

33. Callister, W.D., & Rethwisch, D. G, *Materials science and engineering: An introduction (10th ed.). Wiley.* 2018.

34. Pejkowski, Ł., Seyda, J., Nowicki, K., & Mrozik, D, *Advances in 3D printing materials: Polyethylene terephthalate glycol (PETG) and nylon. Journal of Materials Science & Technology.* 2023.

35. Petousis, M., et al., *The effect of nano zirconium dioxide (ZrO2)-optimized content in polyamide 12 (PA12) and polylactic acid (PLA) matrices on their thermomechanical response in 3D printing.* Nanomaterials, 2023. **13**(13): p. 1906.

36. Kim, H.S., Lee, J. K., & Cho, K., *Stress states in particulate composites. Acta Materialia.* 2000.

37. Chawla, N., & Shen, Y, *Metal matrix composites: An overview. Materials Science and Engineering.* 2001.

38. Ayyar, A., & Chawla, N, *Finite element study of particle morphology and distribution on fracture formation in composite materials. Materials Science and Engineering.* 2006.

39. Popescu, D., & Zapciu, A, *Influence of Process Parameters on FDM 3D Printing Quality. In Advances in Manufacturing, Production Management and Process Control (pp. 261-271). Springer.* 2018.

40. Dutta, D., & Pal, S, *Analysis of Process Parameters in Fused Deposition Modeling. In Additive Manufacturing: 3D Printing for Prototyping and Manufacturing (pp. 57-71). Springer.* 2019.

41. Popescu, D., et al., *FDM process parameters influence over the mechanical properties of polymer specimens: A review.* Polymer Testing, 2018. **69**: p. 157-166.

42. Tofail, S.A.M., & Koumoulos, E. P, *Additive Manufacturing: Innovations, Advances, and Applications. CRC Press.* 2019.

43. Callister, W.D., et al., *Materials science and engineering: an introduction*. Vol. 7. 2007: John wiley & sons New York.

44. Shanmugam, V., et al., *Fatigue behaviour of FDM-3D printed polymers, polymeric composites and architected cellular materials.* International Journal of Fatigue, 2021. **143**: p. 106007.

45. Berde, N.N., Sanap, S. B., & Thorat, S. G., *Study of impact and fatigue on 3D printed composites.* 2021.

46. Ekoi, E.J., A.N. Dickson, and D.P. Dowling, *Investigating the fatigue and mechanical behaviour of 3D printed woven and nonwoven continuous carbon fibre reinforced polymer (CFRP) composites.* Composites Part B: Engineering, 2021. **212**: p. 108704.

47. Şık, A., et al., *Experimental and analytical investigation of the tensile behavior of 3D-printed composites based on micro-CT analysis.* Journal of Thermoplastic Composite Materials, 2023: p. 08927057231211226.

48. Ganeshkumar, S., et al., *Investigation of tensile properties of different infill pattern structures of 3D-printed PLA polymers: analysis and validation using finite element analysis in ANSYS.* Materials, 2022. **15**(15): p. 5142.

49. Dolzyk, G. and S. Jung, *Tensile and fatigue analysis of 3D-printed polyethylene terephthalate glycol.* Journal of Failure Analysis and Prevention, 2019. **19**: p. 511-518.

50. Brackett, D., I. Ashcroft, and R. Hague, *Topology optimization for additive manufacturing.* 2011.

51. Jihong, Z., et al., *A review of topology optimization for additive manufacturing: Status and challenges.* Chinese Journal of Aeronautics, 2021. **34**(1): p. 91-110.

52. Liu, J., et al., *Current and future trends in topology optimization for additive manufacturing.* Structural and multidisciplinary optimization, 2018. **57**(6): p. 2457-2483.

53. Ziemian, S., M. Okwara, and C.W. Ziemian, *Tensile and fatigue behavior of layered acrylonitrile butadiene styrene.* Rapid Prototyping Journal, 2015. **21**(3): p. 270-278.

54. Letcher, T. and M. Waytashek. *Material property testing of 3D-printed specimen in PLA on an entry-level 3D printer*. in *ASME international mechanical engineering congress and exposition*. 2014. American Society of Mechanical Engineers.

55. Gibson, R.F., *Principles of composite material mechanics*. 2007: CRC press.

56. Wang, L., et al., *A multiscale approach for virtual testing of highly aligned short carbon fiber composites.* Composite Structures, 2019. **230**: p. 111462.

57. Chen, J., et al., *High-strength light-weight aramid fibre/polyamide 12 composites printed by Multi Jet Fusion.* Virtual and Physical Prototyping, 2022. **17**(2): p. 295-307.

58. Pertuz, A.D., S. Díaz-Cardona, and O.A. González-Estrada, *Static and fatigue behaviour of continuous fibre reinforced thermoplastic composites manufactured by fused deposition modelling technique.* International Journal of Fatigue, 2020. **130**: p. 105275.